Pore-scale modeling of solute transport in partially-saturated porous media

Ali Saeibehrouzi[1,2], Soroush Abolfathi[2], Petr Denissenko[2], and Ran Holtzman[1]

[1]Centre for Fluid and Complex Systems, Coventry University
[2]School of Engineering, University of Warwick

March 07, 2024

Abstract

Solute transport in partially-saturated porous media plays a key role in multiple applications across scales, from the migration of nutrients and contaminants in soils to geological energy storage and recovery. Our understanding of transport in unsaturated porous media remains limited compared to the well-studied saturated case. The focus of this review is the non-reactive transport driven by the displacement of immiscible fluids, where the fluid-fluid interface acts as a barrier that limits the solute to a single fluid phase. State-of-the-art pore-scale models are described, with a critical analysis of the gaps and challenges. A numerical example is provided to demonstrate the acute sensitivity of solute transport prediction to minute, inevitable uncertainties in the spatial distribution of the fluids' velocities and interface configuration associated with the multiphase flow modeling.

Pore-scale modeling of solute transport in partially-saturated porous media

Ali Saeibehrouzi[a,b], Soroush Abolfathi[b], Petr Denissenko[b], Ran Holtzman[a,*]

[a] *Centre for Fluid and Complex Systems, Coventry University, Coventry, CV1 5FB, UK*
[b] *School of Engineering, University of Warwick, Coventry, CV4 7AL, UK*

Abstract

Solute transport in partially-saturated porous media plays a key role in multiple applications across scales, from the migration of nutrients and contaminants in soils to geological energy storage and recovery. Our understanding of transport in unsaturated porous media remains limited compared to the well-studied saturated case. The focus of this review is the non-reactive transport driven by the displacement of immiscible fluids, where the fluid-fluid interface acts as a barrier that limits the solute to a single fluid phase. State-of-the-art pore-scale models are described, with a critical analysis of the gaps and challenges. A numerical example is provided to demonstrate the acute sensitivity of solute transport prediction to minute, inevitable uncertainties in the spatial distribution of the fluids' velocities and interface configuration associated with the multiphase flow modeling.

Keywords: Solute Transport; Porous Media; Immiscible Fluid displacement; Pore-scale Modeling; Unsaturated Transport; Vadose Zone; Critical Zone Processes; Multiscale Heterogeneity; Multiphase Flow

*Corresponding author

Graphical abstract

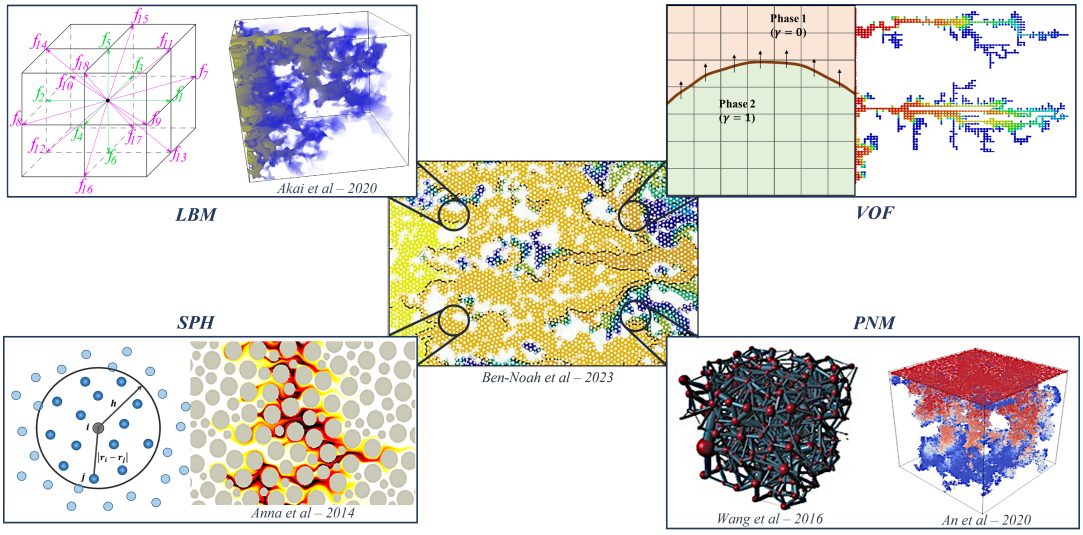

Highlights

- Unsaturated transport is highly sensitive to the fluids' distribution and velocities
- Unsaturated transport is much less understood than its saturated counterpart
- Choice of modeling approach depends on accuracy, computational cost, and application

1. Introduction

Transport of solute in porous materials is ubiquitous in many natural as well as industrial processes. Often, multiple fluid phases co-exist (denoted as "unsaturated' in hydrology, a terminology we adopt here), strongly influencing solute transport within porous media. In the case of immiscible fluids, the fluid-fluid interface serves as a barrier to the transport of solutes, essentially restricting transport to one of the fluid phases. Solute transport driven by immiscible fluid-fluid displacement occurs in a wide range of systems, including soils (e.g. in migration of nutrients and contaminants) and deeper geologic media (e.g. storage of carbon or hydrogen, and contamination from mines or hazardous waste repositories) (Sahimi, 2011; Corada-Fernández et al., 2015; Akai et al., 2020; Bonto et al., 2021).

The displacement of immiscible fluids, the phase distribution and the interface separating them can be highly convoluted and is influenced not only by the fluid properties and flow conditions but also by the underlying porous microstructure (Zhao et al., 2019; Borgman et al., 2019; Wu et al., 2021; Primkulov et al., 2022). The main source of complexity, which make modeling of immiscible fluid displacement challenging, is its multiscale nature: heterogeneity and coupled mechanisms that operate at small scales (below that of single pores) dictate the behavior at the larger scales of interest (Tahmasebi and Kamrava, 2018; Armstrong et al., 2021). A similar challenge exists for solute transport, where recent evidence point to the large extent by which mixing and dispersion are controlled by microscopic mechanisms (Dentz et al., 2011; Heyman et al., 2020; Borgman et al., 2023).

Recent advancements in experimental and computational methods allowed appreciable progress in our understanding of immiscible displacements, as well as of solute transport in a porous medium occupied by a single fluid phase, considered separately (Xu et al., 2017a; Afshari et al., 2018; Watson et al., 2019; Dehshibi et al., 2019; Erfani et al., 2021; Singh et al., 2022). However, our understanding of the coupled process of solute transport driven by immiscible fluid displacements remains partial. A major barrier to our ability to model unsaturated transport in porous media is the sensitivity of the concentration fields to the spatial distribution of the fluid phases and their velocity fields, necessitating detailed knowledge of the flow at very fine scales. Obtaining such information is challenging due to the convoluted fluid-fluid interface and heterogeneous spatial distribution of the fluid phases (Bultreys et al., 2018; Picchi and Battiato, 2018) as well as the strong spatial non-uniformity of fluid velocities, which is further amplified by the presence of multiple fluids (Velásquez-Parra et al., 2022). The coupling of multiple mechanisms across a very wide range of

scales (in particular in geologic media, where processes in nanometric pores can influence km-long reservoirs), leads to a large number of parameters that can span a wide range of values, exacerbating the modeling difficulties.

The aforementioned challenges imply that the selection of the modeling approach for unsaturated transport involves a trade-off between precision, intricacy, and computational expenses (Scheibe et al., 2015a; Meigel et al., 2022). Models for unsaturated transport can be broadly categorized into two types, based on the scale and spatial resolution: (i) pore-scale models—the focus of this review, considering details at the scale of individual pores or smaller (Blunt, 2017); and (ii) continuum (macroscopic) or "Darcy"-scale models, where the basic model unit includes multiple pores, hence the model parameters represent quantities averaged over Representative Element Volumes (REV) containing both pore space and solid matrix, such as porosity and permeability (Mehmani and Balhoff, 2015b). Hence, Darcy-scale models cannot represent pore-scale mechanisms such as thin fingers, snap-off, or flow in films or corners, nor they could capture pressure or concentration gradients below the REV scale. Since unsaturated transport is often controlled by microscopic heterogeneity and mechanisms, pore-scale models are required not only for higher spatial and temporal resolutions but also as means for both fundamental understanding as well as up-scaling and predictive modeling of key macroscopic characteristics such as permeability, capillary pressure, BreakThrough Curves (BTCs), and residence times (Oostrom et al., 2016; Zhang et al., 2019).

Pore scales models can be categorized into two types: Computational Fluid Dynamics (CFD) methods (also denoted at times "direct" methods) that resolve sub-pore transport by discretization of the Navier-Stokes (NS) equations, and Pore Network Model (PNM) where the pore geometry is represented by a network of interconnected simplified geometrical objects (e.g. a network of pipes), allowing to use simplified constitutive rules for fluid and solute transport (e.g. Poiseuille flow) (Joekar-Niasar and Hassanizadeh, 2012; Blunt et al., 2013). CFD methods can be further classified into grid-based versus particle-based. In grid-based models, the flow domain is mapped onto a mesh, and the flow and transport equations are discretized on that mesh using methods such as finite volume or finite difference. In particle-based models, the fluid is represented by a set of discrete particles (Blunt et al., 2013). We review here one grid-based model: (i) Volume of Fluid (VOF), two particle-based methods: (ii) Lattice Boltzmann Method (LBM); and (iii) Smoothed Particle Hydrodynamics (SPH), and also (IV) PNM. PNM, restricted to the level of individual pores, is the most computationally efficient and therefore most suitable for up-scaling, whereas

CFD methods resolve sub-pore flow and transport, allowing simulation of the exact geometry of the porous media. We also briefly review here the so-called multiscale models, in which the flow and transport equations are solved at the Darcy scale in most of the domain and at the microscopic level in domains of special interest.

This review is focused on conservative (non-reactive) solute transport. Since conservative transport can be viewed as a special, degenerate case of reactive transport, we also note recent reviews of pore-scale reactive transport modeling: (i) Mehmani and Balhoff (2015b): an overview with focus on PNM and multiscale models; (ii) Xiong et al. (2016): PNM, emphasizing experimental and analytical methods for pore network construction and characterization; (iii) Soulaine et al. (2021a): briefly reviewing CFD methods (e.g. LBM and SPH), focusing on their implementation in geosciences; (iv) Chen et al. (2022): application of direct methods in natural and industrial processes; (v) Ladd and Szymczak (2021): computational approaches for reactive transport; (vi) Deng et al. (2022): reactive transport for geochemically-driven processes. While there is no benchmark study comparing models against experimental data for unsaturated solute transport, we note several recent relevant studies on related aspects. For solute transport in *saturated* conditions, pore-scale concentrations using both PNM and CFD (LBM and another finite-volume model) compared well with micromodel experiments (Oostrom et al., 2016), and similarly both PNM and LBM were in good agreement with macroscopic breakthrough curves from column experiments (Yang et al., 2016). Immiscible fluid-fluid displacement patterns (with no solutes) obtained from micromodel experiments at a wide range of flow rates and wettability conditions were compared to a large number of models, including PNM, VOF, LBM, as well as Phase Field, Stochastic Rotation Dynamics, and Level Set (not covered here) (Zhao et al., 2019). The authors showed that while all methods were in good agreement with the experiments for a part of the tested conditions, none were able to reproduce the patterns under all conditions. In particular, a challenge to models was flow conditions where partial filling mechanisms dominate, e.g. leading films and corner flow in strong imbibition. This could be achieved by 3D highly-resolved CFD models however at a prohibitive computational cost (e.g. runtime of weeks for LBM using massively parallel machines vs. minutes on a desktop for PNM).

The main objective of this review is to overview the main state-of-the-art methodologies for pore-scale modeling techniques, providing a critical analysis of key challenges and directions for future research. As such, we do not provide a detailed description of these techniques, nor a comprehensive list of publications in which they are presented. We also do not review some techniques such as

Level Set or Phase Field Modeling. The structure of this paper is as follows: Section 2 describes the physical mechanisms and governing equations for multiphase flow and solute transport in porous media. Section 3 reviews the main modeling techniques. Section 4 discusses complexities and pitfalls that are specific to each technique and also describes the main challenges that are common among all methods. This section ends with an exemplification of the sensitivity of unsaturated transport to uncertainties in two-phase displacement. Finally, Section 5 provides concluding remarks.

2. Physical Mechanisms and Governing Equations

In unsaturated transport, solute transport is coupled with the flow of multiple fluids. The flow of two immiscible fluids is controlled by the interplay between viscous, capillary, and gravitational forces, which in turn are affected by the underlying pore structure and the surface properties of the pores (Holtzman, 2016; Borgman et al., 2019; Juanes et al., 2020; Wu et al., 2021). The resulting patterns range from compact displacement, characterized by a stable front that evenly fills the pore space, to highly preferential patterns such as viscous and capillary fingering, involving only a small portion of the pore space (Juanes et al., 2020). When gravitational forces are relatively unimportant (e.g. horizontal flow or very small domain and thus negligible height differences), the flow regime can be characterized by the capillary number, which is the ratio between viscous to capillary forces, $\mathrm{Ca} = \mu_{inv} u_{\mathrm{inv}}/\sigma$, and the viscosity ratio, $\mathrm{M} = \mu_{inv}/\mu_{def}$ (Lenormand et al., 1988). Here, μ_{inv} and μ_{def} are the viscosities of the invading and defending fluids, respectively, u_{inv} is the invading fluid velocity, and σ is the interfacial tension. The relative importance of gravity vs. capillarity is measured through the Bond number, $\mathrm{Bo} = \Delta\rho g R^2/\sigma$, where $\Delta\rho$ is the difference in fluids' density, g is the gravity, and R is the characteristic pore radius (Liu et al., 2013).

The resulting flow field can be divided into three types of regions: isolated, dead-end, and backbone (Ramstad and Hansen, 2006; Khayrat and Jenny, 2016). The backbone zones are the well-connected parts in which the most of flow happens and hence control the flow properties like relative permeability. The dead-end zones do not contribute to fluid flow and act mainly as a sink for the solute, which remains trapped there. Solute transport is mainly controlled by the competition between advection, occurring mostly in the mobile (backbone) regions, and diffusion, which is most effective in immobile (stagnant) zones (Karadimitriou et al., 2017). The interplay between the advection and diffusion is quantified through the Peclet number (Huysmans and Dassargues, 2005), $Pe = \mathbf{u}L/D_m$, where $\mathbf{u}$ is the characteristic velocity of the fluid transporting the solute, D_m is the molecular diffusion coefficient, and L is the characteristic length-scale.

The combination of pore-level diffusion and advection in a heterogeneous medium also gives rise to macroscopic mechanical dispersion (Kulasiri and Verwoerd, 2002; Sahimi, 2012). Therefore, in continuum models with REV containing multiple pores, the macroscopic mass flux of solute is the sum of advective mass flux, diffusive mass flux, and dispersive mass flux, which considers the deviation of pore-level velocity from the macroscopic velocity (Neuman and Tartakovsky, 2009). The dispersion coefficient (D) is the variance of tracer with respect to time (t) as $\sigma^2 = (x_i - \overline{x})^2 = 2Dt$, with x_i being the position of solute particles, and $\overline{x}$ shows the mean solute particles location (De Gennes, 1983; Bijeljic and Blunt, 2006). Another important transport process is mixing, especially when reaction occurs. Mixing affects the probability of tracers (e.g. infiltrated to and resident in porous media) coming into contact and it reduces the likelihood of sharp peaks in tracer concentration (Dentz et al., 2011). While dispersion gives information about the spatial spreading of the tracer and its transfer time within a medium, it does not provide adequate knowledge of the spatial structure of concentration fields (Kitanidis, 1994; Le Borgne et al., 2015). The existence of concentration gradients in a porous structure impacts the mass exchange rate between regions and, as a result, the time evolution of tracer concentration (Hasan et al., 2020).

Unsaturated solute transport can be described by two sets of equations: (i) mass and momentum conservation of the fluids, and (ii) mass conservation for the solute. In the Eulerian framework, the conservation of mass and momentum for each fluid phase i can be written as:

$$\frac{\partial \rho_i}{\partial t} + \nabla \cdot (\rho_i \mathbf{u_i}) = 0 \tag{1}$$

$$\frac{\partial \rho_i \mathbf{u_i}}{\partial t} + \nabla \cdot (\rho_i \mathbf{u_i} \mathbf{u_i}) = -\nabla P_i + \nabla \cdot \left[\mu_i \left(\nabla \mathbf{u_i} + \nabla \mathbf{u_i}^T\right)\right] + \rho_i \mathbf{g} + \mathbf{F_s} \tag{2}$$

where P is the fluid pressure. In the NS momentum Eq. (2), the second term on the left-hand side describes the inertial force. On the right-hand side, the first term is the pressure gradient, the second term is viscous dissipation, the third provides the effect of gravity, and the fourth, $\mathbf{F_s}$, represents interfacial forces. The transport of solute species α (single component with the exclusion of sorption or reaction) is represented by the Advection-Diffusion Equation (ADE):

$$\frac{\partial C_\alpha}{\partial t} + \nabla \cdot (\mathbf{u}\, C_\alpha) - \nabla \cdot (D_{m,\alpha} \nabla C_\alpha) = 0 \tag{3}$$

where C is the species concentration. The first term in Eq. (3) is the temporal evolution of solute, and the second and third correspond to transport via advection and diffusion, respectively. For immiscible fluids, the fluid-fluid interface serves as a barrier to solute transport. As such, it is often

modeled as an impermeable boundary, similar to fluid-solid interfaces. The modeling of both fluid-solid and fluid-fluid interfaces is a subject of debate. Fluid-solid boundaries are typically modeled by a no-slip condition, but this has been shown to be problematic in some cases, for instance, fluids that contain polymers and colloids (Soulaine et al., 2021a), where other approaches like slip models are used to account for non-zero velocity values tangential to the wall. In those models, the magnitude of slippage (i.e. slip length) depends on fluid and surface properties (Ren and E, 2007; Sui et al., 2014). Comparison between no-slip and free-slip conditions in recent investigations have also revealed that applying no-slip conditions for fluid-fluid interfaces has a minimal effect on solute migration (Guédon et al., 2019; Triadis et al., 2019).

In many cases, the timescale for immiscible fluid displacement required to reach steady-state conditions, in terms of fluids configurations and velocities, is much shorter than the timescale of solute transport. This could be modeled as one-way coupling, where solute transport in the "carrier" fluid phase is modeled by considering the final (steady-state) fluid configuration, disregarding solute transport during the transient flow when interface evolution by pore invasion occurs (Jimenez-Martinez et al., 2015; Karadimitriou et al., 2016, 2017; Aziz et al., 2018, 2019; Hasan et al., 2019; Aziz et al., 2020; Gong and Piri, 2020). This provides a substantial simplification compared to the full two-way coupling of fluid displacement and solute migration that occurs during the short transient stage and thus is frequently used in both experimental and computational investigations. Furthermore, in this one-way coupling approach, predetermined fluid configurations obtained experimentally could be employed in numerical simulations without simulating their evolution (which is the most computationally demanding step) (Ben-Noah et al., 2023). Such steady-state configurations could also serve as training data for machine learning, facilitating the analysis of other conditions (Jimenez-Martinez et al., 2020).

3. Models for Unsaturated Transport

3.1. Volume of Fluid

Fluid displacement. VOF method is a broadly recognized grid-based technique for accurately capturing the interface between fluids. Originally developed for viscous-dominated flows, it has since been extensively utilized in CFD applications, particularly in pore-scale modeling (Maes and Geiger, 2018; Rabbani et al., 2018; Ambekar et al., 2021a,b; Yang et al., 2021c). The phase occupancy in each modeling cell in terms of volumetric fraction (called "volume indicator" or "marker function", γ) is

$$\gamma = \begin{cases} 0 & \text{for } \Omega_1 \quad \text{(Phase 1)} \\ [0,1] & \text{for } \Gamma \quad \text{(Interface)} \\ 1 & \text{for } \Omega_2 \quad \text{(Phase 2)} \end{cases} \tag{4}$$

For a system with n phases, $n-1$ indicator functions are required to determine the interfaces. The interface evolution in time is described through an advection equation

$$\frac{\partial \gamma}{\partial t} + \nabla.(\gamma \mathbf{u}) = 0 \tag{5}$$

which is coupled with the NS equations for the conservation of mass and momentum, providing the velocity fields $\mathbf{u}$. Two primary techniques can be employed to determine the configuration of the interface : (i) Algebraic, where the interface is tracked by directly solving the advection Eq. (5); and (ii) Geometric, which explicitly reconstructs the interface by utilizing a geometric representation (such as a quadratic surface) (Maes and Soulaine, 2018). In general, while both techniques share the advantage of mass conservation, the Geometric VOF method outperforms the Algebraic method in minimizing interface numerical diffusion at the expense of a more complex implementation for unstructured cells (Jamshidi et al., 2019).

In the Algebraic formulation, the curvature of the interface κ can be found through the gradient of the indicator function:

$$\kappa = -\nabla \cdot \mathbf{n} = -\nabla \cdot \frac{\nabla \gamma}{|\nabla \gamma|} \tag{6}$$

where $\mathbf{n}$ is unit normal vector of interface. The interfacial forces in the NS equation can be calculated by the Continuum Surface Force (CSF) (Brackbill et al., 1992):

$$\mathbf{F_s} = \sigma \kappa \nabla \gamma \tag{7}$$

The volume-weighted fluid properties at the interface are calculated by

$$\begin{aligned} \rho &= \gamma \rho_1 + (1-\gamma)\rho_2 \\ \mu &= \gamma \mu_1 + (1-\gamma)\mu_2 \end{aligned} \tag{8}$$

For further details of other variants of VOF and their implementation refer to Gopala and van Wachem (2008); Bilger et al. (2017); Pavuluri et al. (2018).

Solute transport. The ADE can be employed directly to simulate solute transport in grid-based techniques (Dou et al., 2022; Noughabi et al., 2023). A common approach to substantially reduce computing time while still conserving solute mass within the carrier phase and avoiding its

migration through fluid-fluid boundaries is to generate a numerical domain based on the carrier phase distribution. With this, only the velocity field (single-phase) in the carrier phase needs to be calculated, whereas, in terms of solute transport, the second fluid phase is treated similarly to the solid phase i.e. with no-flux boundary conditions. This scenario is valid for laminar flow in porous media when the solute solution's injection rate in the carrier phase is small enough that it cannot significantly alter the fluid-fluid boundaries (Jimenez-Martinez et al., 2020; Ben-Noah et al., 2023). Another approach to account for zero diffusive mass flux between the two fluid phases is by introducing three phases that are transported: (i) invading (carrier) fluid phase, (ii) defending fluid phase, and (iii) infiltrated phase that mixes with the invading phase and acts as the solute solution (Aziz et al., 2020). An additional diffusion coefficient between infiltrated and defending phases is included in the modeling to avoid solute migration from the invaded fluid to the defending fluid. This is achieved by setting this additional coefficient to zero, generating a no-flux boundary condition for the tracer between the carrier and defending phases.

3.2. Lattice Boltzmann Modeling

In LBM, each fluid is represented by a group of particles, carrying averaged properties such as density and momentum. Flow is simulated by fluid particles motion and collision on a computational grid, through particle distribution functions. The simulated flow at near-incompressible conditions in LBM provides a close approximation of the NS equations. The method is highly suitable for parallel computing for the simulation of media with irregular pore shapes, and it can automatically handle phase separation by tracking the particles of each phase. Particles' motion is computed by discretizing the Boltzmann equation, restricting the motion of particles in each time step to a limited number of discrete locations on a lattice (Coreixas et al., 2019). The lattice configuration is indicated by $\mathrm{D}_n\mathrm{Q}_m$, in which n denotes the dimensions of simulation (2D or 3D) and m is the number of directions (Fan et al., 2019; Wang et al., 2019), see Fig. 1.

Fluid displacement. The general form of the LBM equation can be written as

$$f_i(x + e_i\delta t, t + \delta t) - f_i(x, t) = \Omega_i \tag{9}$$

where $f_i(x,t)$ is the distribution function indicating the probability that particles located at the lattice site x at the time t moves in the direction i, e_i denotes the particle discrete velocity, and Ω_i corresponds to the collision operator, describing the intermolecular interactions. The left-hand

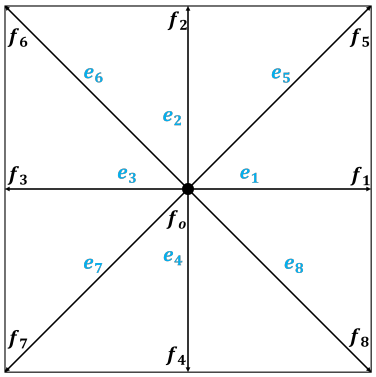

Figure 1: An example of lattice arrangement and velocity distribution for a D_2Q_9 LBM.

side of Eq. (9) is called "streaming step", and the right-hand side "collision step" (He et al., 2019; Ramstad et al., 2019).

The fluid density and velocity at position x and time t are determined by the distribution function as follows:

$$\rho(x,t) = \sum_i f_i(x,t) \tag{10}$$

and

$$u(x,t) = \frac{1}{\rho(x,t)} \sum_i e_i f_i(x,t) \tag{11}$$

Pore walls are introduced as immobile solid particles that stop fluid particles penetration across and propagation along the wall via no-flow and no-slip boundary conditions, by mirroring particle momentum when it collides with a solid surface ("bounce-back") (Golparvar et al., 2018; Ramstad et al., 2019).

Different LBM variants exist for multiphase flow, including pseudopotential or Shan-Chen model (Shan and Chen, 1993, 1994), color-gradient model (Gunstensen et al., 1991; Tolke et al., 2006), and the free energy model (Swift et al., 1996). Among these, the pseudopotential and color-gradient are more common for porous media. The major difference among them is the way that phase separation is simulated. For each phase α, a different distribution function is introduced, such that $f_i(x,t) = \sum_\alpha f_i^\alpha(x,t)$. The color-gradient model is advantageous for multiphase flow due to its ability to set phases viscosity ratio and interfacial tension independently (Bakhshian and Hosseini, 2019; Chen et al., 2019; Liu et al., 2021). The pseudopotential model aims to simulate the microscopic interactions between the nearest fluid particles by introducing an effective mass. While it is known for its simplicity and computational efficiency, the model may require some pre-processing of input parameters in certain scenarios (see section 4.1.2) (Liu et al., 2021). For further

information regarding the implementation of LBM in multiphase flow see recent reviews by Chen et al. (2014); Liu et al. (2016); Coreixas et al. (2019); Liu et al. (2021).

Solute transport. Unlike the flow described by the nonlinear NS equations, the ADE is linear in velocity, indicating that linear equilibrium distributions can be used. This results in a lower number of lattice directions, such that for instance D_2Q_9 and D_3Q_{17} schemes for flow reduce to D_2Q_5 and D_3Q_7 for transport, respectively. The migration of solute component k is represented by concentration distribution functions (Sullivan et al., 2005; Chen et al., 2012; Zhou et al., 2015; Chen et al., 2018a; Zhang et al., 2021):

$$g_{i,k}(x + e_i\delta t, t + \delta t) - g_{i,k}(x,t) = -\frac{g_{i,k}(x,t) - g^{eq}_{i,k}(x,t)}{\tau_C} \tag{12}$$

where τ_C is relaxation time indicating the time rate, and

$$g^{\mathrm{eq}}_{i,k} = C_k\omega_i\left[J_{i,k} + \frac{e_i \cdot \mathbf{u}}{c_s^2}\right] \tag{13}$$

is the equilibrium distribution function, with $C_k = \sum g_{i,k}$ and J_i can be defined as (e.g. for D_2Q_5):

$$J_i = \begin{cases} J_0, & i = 0 \\ (1 - J_0)/4, & i = 1,2,3,4 \end{cases} \tag{14}$$

Here, J_0 is the rest function ranging between 0 to 1, corresponding to different diffusivity, c_s is the lattice speed of sound, and ω_i is a weighting factor. The relation between lattice diffusion coefficient and relaxation time in 2D is given by

$$D_m = \frac{1}{2}(1 - J_0)(\tau_C - 0.5) \tag{15}$$

In modeling multiphase flow, Chen et al. (2013) presented a model to account for zero concentration flux between phases through a critical density within the system; if a node's density is greater than that value, it is considered a carrier-phase node, and otherwise, it belongs to the other phase. While effective in closed systems (e.g. brine inclusion in a crystal of salt subjected to thermal gradient), this technique is associated with high computational costs and requires the redistribution of solutes to preserve mass conservation (Li and Berkowitz, 2019).

Another approach to include the effect of fluid-fluid interfaces on solute migration was developed by Riaud et al. (2014) and Zhao et al. (2015) for the color-gradient model through the modification of the collision operator of species, resulting in the following equilibrium distribution function

$$g_{i,k}(x + e_i\delta t, t + \delta t) - g_{i,k}(x,t) = -\frac{g_{i,k}(x,t) - g^{eq}_{i,k}(x,t)}{\tau_C} + \beta_k W(x_r)\, g^{eq(0)}_{i,k}\frac{e_i \cdot n}{\|e_i\|} \tag{16}$$

where, $g_{i,k}^{eq(0)} = \omega_i C_k$, n is normal to the interface, $W(x_r)$ is an arbitrary function that acts as a driving force on solute solution, and β_k tunes the profile of interface and relates the diffusion coefficient to the relaxation time. For a two-phase scenario, while solute is only migrated in one phase, the single driving force can be chosen such that $W(x_r) = -(1 - x_r)$. Here, x_r is the concentration fraction in the carrier phase, such that for $x_r = 1$ solute diffuses in the carrier phase, and for $x_r = 0$ the second phase repels the solute.

Unsaturated solute transport can also be simulated in the Shan-Chen LBM method by considering three types of particles ("fluids"): two *resident* fluids, Ω_1 (carrier) and Ω_2 (corresponding to the two physical immiscible fluids), where the solute is represented by an "*infiltrated* fluid" Ω_3 that mixes with the carrier fluid (Li and Berkowitz, 2018; Zhao et al., 2021). To that end, the interaction coefficient between mixing fluids particles in the collision operator (Eq. (17)) is reduced significantly below the critical phase separation value. The mixing of infiltrated fluid with the other (non-carrier) fluid is avoided by increasing the interaction coefficient above the threshold (Li and Berkowitz, 2018).

$$\mathbf{F}_{inter,\alpha} = -G_c \psi_\alpha(\mathrm{x}, t) \sum_{\beta \neq \alpha} \sum_{i=1} \omega_i \psi_\beta \left(x + e_i \Delta t, t\right) e_i \tag{17}$$

Here, α and β represent phases, ψ is the effective mass density of the fluid, and G_c is the interaction coefficient adjusting the cohesion forces between two components (α and β) with positive values for repelling particles and negative values for cohesive forces.

3.3. Smoothed Particle Hydrodynamics

SPH was initially developed for compressible fluids in astrophysics and later was extended to incompressible free-surface flows, such as a dam break problem (Monaghan, 1994). SPH is a mesh-free, particle-based Lagrangian approach representing fluid flow as multiple interacting particles possessing a given volume and mass. Particles act as discretization points to solve the governing (NS) equations. Similar to the particle-based LBM, the SPH does not require handling phase boundaries explicitly, allowing the natural account of complex geometries and boundaries. However, it is more computationally demanding than Eulerian, grid-based techniques as SPH requires a much higher number of particles than grid points in Eulerian methods for the discretization of the spatial term (Tartakovsky et al., 2016; Bui and Nguyen, 2021).

Fluid displacement. In SPH, any tensor or scalar property $A(x)$ is formulated by integral interpolation (Kunz et al., 2016; Peng et al., 2017; Wu et al., 2020),

$$A(x) = \int A(x')W(x - x', h)\, dx' \tag{18}$$

represented in discretized form, known as particle approximation of $A(x)$ as:

$$A_i(x) = \sum_{j=1}^{N} \frac{m_j A_j(x)}{\rho_j} W_{ij} \tag{19}$$

where indices i and j count for particles, N is the number of the particles inside the support territory of reference particle i, m is the particle mass, W is the kernel function (a weighing function with the dimension of inversed volume), x is the distance, and h is the smoothing length, indicating the affecting region of the kernel function, see Fig. 2. Similar to Eq. (19), one can employ the following

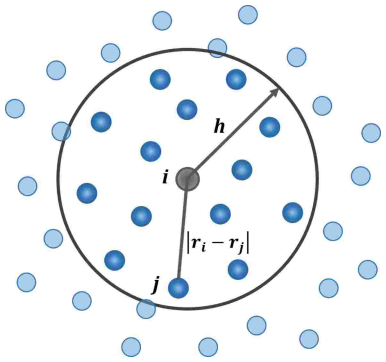

Figure 2: Fluid particles inside the Kernel function smoothing length h for particle i in SPH.

expression inside a sampling volume to determine the gradient of a continuous function:

$$\nabla A_i(x) = \sum_{j=1}^{N} \frac{m_j A_j(x)}{\rho_j} \nabla W_{ij} \tag{20}$$

The NS momentum equation in the Lagrangian form is written as:

$$\frac{d\left(\rho_i \mathbf{u}_i\right)}{dt} = \left(-\nabla P_i + \nabla \cdot \left[\mu_i \left(\nabla \mathbf{u_i} + \nabla \mathbf{u_i}^T\right)\right]\right) + \mathbf{g} + \mathbf{F_s} \tag{21}$$

Eqs. (19–20) can be used to approximate the NS momentum equation, e.g. $\nabla P_i = \sum_{j=1}^{N} \frac{m_j P_j}{\rho_j} \nabla W_{ij}$, resulting in a system of ordinary differential equations (Monaghan, 2005; Tartakovsky et al., 2009; Yang et al., 2020):

$$\frac{d\left(m_i \mathbf{u}_i\right)}{dt} = F_i + F_i^{interaction} \tag{22}$$

where F_i is the total force affecting particle i (that is pressure force, viscous force, body force, excluding interfacial force) and $F_i^{interaction}$ is the force acting on particle i owing to interactions with the other phases, (known as pairwise interaction model) $F_i^{interaction} = \sum_{j=1}^{N} F_{ij}$ where

$$F_{ij} = \begin{cases} s_{ij} \cos(\frac{1.5\pi}{h} |\mathbf{x_i} - \mathbf{x_j}|) \frac{\mathbf{x_i} - \mathbf{x_j}}{|\mathbf{x_i} - \mathbf{x_j}|}, & \text{for } |x_j - x_i| \leq h \\ 0, & \text{for } h < |x_j - x_i| \end{cases} \tag{23}$$

Here, s_{ij} is the "interaction strength" between two particles, which represents the wetting condition and the interface contact angle, set by adjusting the relative ratio of interaction coefficients between particles of the same phase ($i = j$) and different phases ($i \neq j$). In addition to the above-mentioned definition of interfacial forces, there are other forms and readers can refer to a review by Wang et al. (2016b) for more information.

Similar to fluids, solid boundaries are represented by particles. To enforce no-flow boundaries, particles that are repulsive to the fluids can be placed (Monaghan, 1994). Another approach for considering solid boundaries is "ghost" particles, located outside the fluid but mirroring fluid particles' properties along the boundary (the perpendicular component of velocity for ghost particles is of opposite sign to fluid particles). Depending if a slip or no-slip condition is enforced, the same or the opposite sign needs to be assigned to the tangential velocity component, respectively. For this approach, the location of reflected particles is usually fixed in time, i.e. the velocity component is found from fluid particles according to the distance between them (Morris et al., 1997; Liu et al., 2012). One overarching challenge in imposing boundary conditions in SPH is the length of the support domain for the kernel function that may be overlapped or truncated with the boundary. For more details regarding the implementation of SPH for single and multiphase flows see Tartakovsky and Meakin (2006); Tartakovsky et al. (2009, 2016).

Solute transport. SPH naturally provides a physical representation of advection and diffusion, and thus has been used extensively to model transport in porous media (Tartakovsky et al., 2007a,b; Ryan et al., 2011; De Anna et al., 2014; Yang et al., 2021a). The ADE can be written in the moving Lagrangian system formulation as (Zhu and Fox, 2001; Meakin and Tartakovsky, 2009):

$$\frac{dC}{dt} = \frac{1}{\rho} \nabla (D_m \rho \nabla C) \tag{24}$$

which for particle i results in (Meakin and Tartakovsky, 2009; Ryan et al., 2011):

$$\frac{dC_i}{dt} = \frac{1}{m_i} \sum_{j \in \text{ fluid}} \frac{(D_{m,i} n_i m_i + D_{m,j} n_j m_j)(C_i - C_j)}{n_i n_j (\mathbf{r}_i - \mathbf{r}_j)^2} (\mathbf{r}_i - \mathbf{r}_j) \cdot \nabla_i W(\mathbf{r}_i - \mathbf{r}_j, h) \tag{25}$$

where C_i is the solute concentration (the ratio between the mass of solute carried by particle i to the mass of solution carried by particle i), $D_{m,i}$ is diffusion coefficient associated with particle i, and n is particle number density (density to mass ratio). The separation of phases between fluids (e.g. particles representing solute in one phase) is implemented by adjusting the interaction forces between particles. This is accomplished by indicating the interaction strength s_{ij} in Eq. (23) between particles of the same fluid to be higher than for particles of different fluids (Tartakovsky and Meakin, 2006; Tartakovsky et al., 2009).

3.4. Pore Network Modeling

PNM was developed by Fatt (1956), solving for flow (mass conservation) by a set of equations akin to Kirchhoff's using an analogy between a network of tubes and electrical resistors. In PNM, the intricate pore geometry is replaced by a set of interconnected pores with simplified geometry, which allows the use of analytical expressions for capillary entry pressure and the averaged fluid velocity. One common example used for multiphase flow is discretizing the pore space into "pore bodies" containing most of the fluid volume, interconnected by constrictions or "throats" (usually of cylindrical shapes) where most of the pressure drop occurs which thus controls the velocity. Another common variant is a network of cylindrical tubes which contain all the volume, connected at nodes or pore junctions where the conservation equations are enforced (for fluid momentum and solute mixing). A pore network can be generated directly from a specific sample by discretizing a complex porous volume, e.g. using X-ray microtomography, or in a statistical sense, maintaining features such as pore size distribution, connectivity, and topology (Bultreys et al., 2016; Wang et al., 2016a; Lai et al., 2018). PNM provides a trade-off between accuracy and computational efficiency, simplifying the pore geometry in a way that still captures the essential physical mechanisms including some of the essential (statistical) features of the pore geometry. This enables simulations of much larger domains than other pore-scale methods, hence allowing both introduction of various types of heterogeneity as well as repeated realizations (Mehmani and Balhoff, 2015b; Borgman et al., 2019).

Fluid displacement. The most simple implementation of PNM for fluid flow is for quasi-static fluid-fluid displacement, using the Invasion-Percolation (IP) model (Wilkinson and Willemsen, 1983). This assumes instantaneous pore filling through a series of local jumps or bursts, relying on the separation of timescales between Haines jumps and the macroscopic driving force of the invasion (such as injection rate or changes in pressure). These models also rely on instant

relaxation of pressures following an invasion event, which makes these events independent in space. Consequently, the pressure between invasion events is considered spatially uniform, and the displacement pattern depends solely on the pore topology (spatial arrangement of capillary entry pressures) (Blunt, 2001; Golparvar et al., 2018; Biswas et al., 2018). Pore invasion occurs once the local capillary pressure exceeds the entry threshold, computed from the Young-Laplace rule for complete pore filling. The case of partial pore filling e.g. film and corner flows requires more intricate criteria (Primkulov et al., 2018; An et al., 2020a).

To relax the assumption of quasi-static displacement, "dynamic PNM" introduces the effect of viscosity and pore pressure dissipation by resolving the temporal evolution of the pressure field, hence requiring higher computational cost (Aker et al., 1998; Holtzman and Juanes, 2010; Joekar-Niasar and Hassanizadeh, 2012; Aghaei and Piri, 2015). For incompressible flow, pressures and velocities are resolved from the continuity equation (akin to Kirchhoff's law), which for pore i reads

$$\sum_{j=1}^{N_i} q_{ij}^{\alpha} + q_{ij}^{\beta} = 0 \tag{26}$$

Here N_i is the total number of pores j connected to the pore i. The flow rate between pores i and j for phase α, neglecting gravity and fluid compressibility, can be determined by the Hagen-Poiseuille equation (Sun et al., 2016; Borgman et al., 2019):

$$q_{ij}^{\alpha} = \frac{F_{ij}^{\alpha}}{L_{ij}}(P_{i,\alpha} - P_{j,\alpha}) \tag{27}$$

where L_{ij} is the distance between pore centers, and F_{ij}^{α} denotes the fluid conductance for phase α, computed from the shape of the conduit connecting pore i to j, and fluid viscosity. Gravity can be introduced by using a potential as the driving force instead of the pressure P. The pressure field in the entire domain results in an algebraic system of equations at each time step. For the compressible case, the volumetric flux leaving pore i and entering pore j do not cancel, and Eq. 26 needs to be revised to account for compressibility (Huang et al., 2016). For more details on PNM for single and multiphe conditions see Joekar-Niasar and Hassanizadeh (2012); Xiong et al. (2016); Hosseinzadegan et al. (2023).

Solute transport. PNM typically considers a single (volume-averaged) value for velocity, pressure, and concentration in each unit volume (pore), which in the context of solute transport is denoted the Mixed-Cell Method (MCM). MCM relies on perfect mixing within each pore (Hasan et al.,

2019). With that, the discrete solute conservation equation is:

$$V_i \frac{dC_i}{dt} = \sum_{j=1}^{N_i^{\text{th. }, q<0}} C_i q_{ij} + \sum_{j=1}^{N_i^{\text{th }, q>0}} C_j q_{ij} + \sum_{j=1}^{N_i^{\text{th}}} D_{\text{m}} A_{ij} \frac{C_j - C_i}{L_{ij}} \qquad \{i,j\} \in \Omega_{\text{carrier phase}} \tag{28}$$

where V is pore volume and A is the cross-section area.

The well-mixed assumption in MCM provides a good approximation for low Pe where diffusion dominates over advection, smoothing the pore-scale concentration gradients (Mehmani and Balhoff, 2015b). PNM for solute transport can also be used in a Lagrangian framework, denoted Particle Tracking Method (PTM). In PTM, the motions of solutes (represented by non-interacting particles) are tracked using the velocities obtained from Eularian PNM described earlier (Bijeljic and Blunt, 2007). PTM typically represents pore geometry as a network of tubes (mixing in the nodes) (Vasilyev et al., 2012; Meng and Yang, 2019). Hence, PTM and MCM often rely on different network extraction method (Acharya et al., 2007). PTM, being particle-based, is more precise but more computationally intensive than grid-based PNM e.g. MCM (Mehmani and Tchelepi, 2017).

3.5. Multiscale Methods

Computational cost makes the application of pore-scale models (in particular CFD) prohibitive for large domains, e.g. field scale. Multiscale models aim to address this challenge by solving the flow and transport equations at different spatiotemporal resolutions. Below we describe two such methods; more detailed discussions can be found e.g. in Yang et al. (2021b); Mehmani et al. (2021).

Micro-Continuum Method (Filtering). This approach is based on the Darcy-Brinkman-Stokes (DBS) equation, obtained by integrating the NS equation over a REV containing both fluid and solid phases (Brinkman, 1949). In regions with fluids only, where the drag force vanishes, the DBS equation is equivalent to the NS equation, and elsewhere it becomes a Darcy-like equation (Soulaine and Tchelepi, 2016; Soulaine et al., 2021b). Fig. 3 shows domain discretization for the micro-continuum approach and its comparison with pore- and Darcy-scale modeling. Analogous to the DBS equation, a volume-averaged ADE is used to model transport:

$$\frac{\partial \varepsilon_f \overline{C}_f}{\partial t} + \nabla \cdot \left(\overline{\boldsymbol{u}}_f \overline{C}_f \right) = \nabla \cdot \left(\varepsilon_f \boldsymbol{D_m} \nabla \overline{C}_f \right) \tag{29}$$

where ε_f is porosity, and $\overline{C}_f$, $\overline{\boldsymbol{u}}_f$ are averaged concentration and velocity, in turn.

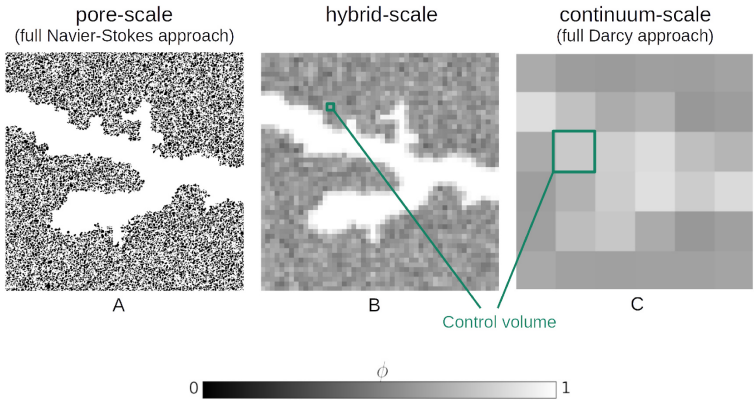

Figure 3: Domain discretization and porosity (ϕ) distribution at (A) pore-scale approach, where white is the void space and gray is the solid wall, (B) filtering approach used in the micro-continuum method, where a cutoff length is indicated according to the REV, and (C) macro-scale approach, where all control volume can contain both solid and fluid phase (Soulaine et al., 2021b). Note that the indicated control volume in the hybrid- and macro-scale represent regions with different sizes for a distinct approach.

Hybrid Multiscale Method (domain decomposition). A general technique that allows the use of different pore-scale models in regions of interest embedded in a larger domain where a continuum, Darcy-scale model is implemented (Yang et al., 2021b; Scheibe et al., 2015b). A scale coupling condition (a bilateral communication) is implemented for the interface of discretized subdomains to assure the continuity of fluxes and concentration fields over the macro- and pore-scale regions (Roubinet and Tartakovsky, 2013).

4. Discussion: Modeling challenges

As said, each approach has its advantages and disadvantages in terms of computational cost and precision. In this section, we examine the challenges, shortcomings, and proposed resolutions specific to the reviewed methods, followed by a discussion of the more general challenges (not specific to one method). We end with an example showing the high sensitivity of transport modeling to uncertainties in multiphase flow details.

4.1. Model-specific challenges

4.1.1. Volume of Fluid

One of the most pervasive issues in the simulation of multiphase flows, in particular, slow flows of high-density contrast, is spurious vortex-like currents, also known as parasitic currents. These result from the inaccuracy in the discretization of the pressure gradient and surface tension in

Eq. (2), and improper determination of interface curvature (Popinet, 2018). These artificial currents add additional viscous dissipation and shear stress, which in turn lead to inaccurate estimation of displacement pattern (Pavuluri et al., 2018). This makes implementation of VOF in slow (low Ca) cases challenging (Jamshidi et al., 2019). For instance, the commonly used VOF-CSF, describing interfacial forces, is often associated with strong spurious currents (Hu et al., 2017; Rabbani et al., 2016, 2018; Ambekar et al., 2021a). Alternatives methods for CSF that improve the interfacial forces and curvature in different ways include the Sharp Surface Force (SSF) method (Francois et al., 2006), Filtered Surface Forces (FSF) method (Raeini et al., 2012), and Contour-Level Surface Force (CLSF) (Shams et al., 2018). SSF smooths the indicator function, which is successful in reducing parasitic currents in the quasi-static case but not efficiently in dynamic cases. FSF addresses that by separately solving for the dynamic (viscous) and capillary forces, removing the parasitic currents that are parallel to the interface. This is achieved by modifying the capillary forces that are accountable for those currents. The CLSF employs a sharp iso-contour surface to indicate the interface and define it as discrete elements, providing a good representation of the interface with marginal spurious currents even at low mesh density. FSF is more efficient for diminishing the spurious velocities (compared to SSF and CSF), yet requires extra heuristic parameters and suffers from periodic bursts in velocity fields that affect the advection of the interface (Pavuluri et al., 2018; Yang et al., 2021c).

Another resolution is to combine VOF with other interface models. For instance, Level Set, an Eulerian method (not covered in this review), can be used to calculate the interface configuration, which is then used in VOF when solving interface advection (Albadawi et al., 2013; Peyman and Apostolos, 2016; Haghshenas et al., 2017; Cao et al., 2020). This approach exploits the advantages in both methods: mass conservation in VOF and a sharp interface in Level Set, which results in reduced spurious currents however at a much higher computational cost (Hoang et al., 2013; Dianat et al., 2017).

4.1.2. Lattice Boltzmann Modeling

In general, the accuracy of LBM in simulation can be enhanced by increasing the lattice resolution (number of directions), however with an increase in computational cost (Kang and Hassan, 2013; Kuwata and Suga, 2015; Liu et al., 2021). Nevertheless, at some conditions, lower resolution in terms of lattice directions has been shown to perform better; for instance, while D_2Q_9 lattice suffered from smaller errors vs. the coarser D_2Q_5 at high Pe, the opposite was found for lower Pe.

Similar findings were also shown in 3D (D_3Q_7 vs. D_3Q_{19}) (Li et al., 2017).

A pervasive challenge in multiphase LBM (especially the pseudopotential method) is representing fluids of high density and/or viscosity ratios (Molaeimanesh and Akbari, 2016; Huang et al., 2020). This is particularly the case for simulation with a simple scheme for the collision operator (known as Single Relaxation Time (SRT)). A collision operator known as Multi Relaxation Time (MRT), improving upon SRT, has been suggested as a solution to improve the performance and stability of the model.

The color-gradient LBM method uses a fictitious density to capture the effect of the contact angle (Latva-Kokko and Rothman, 2005), which was found to introduce numerical mass transfer along the solid-fluid interfaces (Leclaire et al., 2016; Akai et al., 2018). For a restricted range of contact angles, this was alleviated by introducing the static contact angle as a Dirichlet boundary condition in 2D and 3D (Leclaire et al., 2016, 2017). Another scheme to improve modeling wetting phenomena and reduce spurious currents for the color-gradient approach was introduced by Akai et al. (2018) (extending the geometrical method in Xu et al. (2017b) to 3D). The method works based on enforcing the color-gradient's direction to match the required contact angle on the solid boundary. However, this scheme uses the SRT scheme, which can cause numerical instabilities.

In the pseudopotential method, determining the interaction coefficient G_c in modeling the phase separation or mixing (Eq. 17) is a cumbersome step. A stability analysis to test its value is required to ensure that it is sufficiently high for phase separation between the fluids (strong repulsive forces), and sufficiently low for numerical stability (Huang et al., 2007; Ikeda et al., 2014).

Enforcement of the boundary conditions at fluid-solid interfaces is another challenging aspect. The bounce-back scheme's accuracy is highly influenced by the spatial location of solid and fluid nodes and their proximity to the wall interface (Yin and Zhang, 2012). In addition, the type of incorporated collision operator can also affect the performance of wall treatment in LBM. For instance, employing the SRT collision operator with the bounce-back scheme may cause errors in modeling and result in viscosity-dependent permeability. Various schemes have been introduced for representing boundaries according to spatial interpolations methods between solid and fluid nodes, however, they can be prohibitive in terms of computational power and numerical stability (Yoon et al., 2015; Ramstad et al., 2019).

4.1.3. Smoothed Particle Hydrodynamics

A fundamental challenge in SPH (and other particle-based techniques) is modeling the hydrodynamic force arising from the merging of fluid interfaces, as it requires a high number of model particles (TingYe et al., 2019). One method to consider interfaces interactions was proposed by Hirschler et al. (2017) that is based on the energy model, relating the surface energy to the kinetic energy. The model works based on a critical Weber number (relative importance of inertia to surface tension) to accounts for droplets' transition from bouncing to coalescence. Another approach based on CSF for calculating interfacial forces is using a film drainage model that allows trapped particles between two interfaces to drain out (Rahmat and Yildiz, 2018).

A common difficulty in the SPH is the modeling of solid boundaries. For instance, in the repulsive solid boundary model, an improper cut-off distance (length at which solid particles start interacting with fluid particles) can cause either nonphysical penetration of fluid particles into the solid wall or pressure oscillations. The ghost particles method works well, however, only for simple geometry, and indicating the ghost particles' velocity and location in complex boundaries is elusive (Holmes et al., 2011; Liu et al., 2012; Tartakovsky et al., 2016; Wang et al., 2016b).

Another unresolved issue in SPH is imposing prescribed flow and pressure boundary conditions. Periodic boundary condition, commonly used in SPH, does not work well in complex flow fields, for instance, where inlet and outlet geometries are not aligned (Morris et al., 1997; Zhu and Fox, 2002; Jiang et al., 2007; Tartakovsky et al., 2009). Different studies tried to address this issue and impose prescribed velocity filed for flowing boundaries (Lastiwka et al., 2009; Hosseini and Feng, 2011; Federico et al., 2012; Kunz et al., 2016). These new developments, however, faced challenges such as disagreements between numerical and experimental results or problems in modeling cases when flow regimes in transient conditions are needed (Holmes and Pivonka, 2021).

4.1.4. Pore Network Modeling

Although the included simplifications in PNM result in reduced computational cost, the fact that these simplifications can cause errors in capturing flow and transport properties has motivated researchers to further improvement of PNM. Efforts have been given to, for instance, combine PNM with other CFD techniques to solve flow equations (Rabbani and Babaei, 2019; Montellá et al., 2020; Lanetc et al., 2022) or employ machine-learning algorithms for finding throat conductance (Miao et al., 2017).

Extraction of the pore network remains a major challenge and distinguishing the pore and

throat space for the network extraction algorithm is not straightforward (Joekar-Niasar, 2016). For instance, Bhattad et al. (2011) highlighted the high sensitivity of estimated capillary pressure curves from quasi-static PNM to the variation in pore network topology. Network extraction becomes even more challenging in the presence of multiscale heterogeneity, common in e.g. carbonates and fractured rocks. Evaluating parameters such as relative permeability and capillary pressure are based on the assumption of well-connected pores on a single scale (Mehmani et al., 2020). This motivated the development of two-scale (macro- and micro-porosity) PNM, where networks at more than one pore level are coupled (Jiang et al., 2013; Mehmani and Prodanović, 2014; Bultreys et al., 2015). Jiang et al. (2013) presented a numerical construction algorithm for combining generated networks from CT images of different length scales. Mehmani and Prodanović (2014) developed a two-scale network generation approach by using the Delaunay tessellation of grain centers to form the macro network. Intraparticle void space, i.e. micro networks, were generated based on a scaling factor and down-scaling extracted macro network. An image-based method was presented by Bultreys et al. (2015) for incorporating networks at different length scales by considering micro-porosity as a continuous medium. The proposed algorithms by Jiang et al. (2013) and Bultreys et al. (2015) exclude the effect of micropores that cannot be captured by micro-CT and ignores geometric details of micropores clusters. The developed method by Mehmani and Prodanović (2014) produced distorted pores for the cases when a large grain is in contact with finer grains (Xiong et al., 2016).

For solute transport, various improvements to MCM have been proposed, including assigning volumes to and solving for concentrations in both pores and throats or using a modified diffusion coefficient (Raoof and Hassanizadeh, 2013; Seetha et al., 2017; Gong and Piri, 2020). For instance using an effective pore-wise molecular diffusion which accounts for Taylor-Aris dispersion within throats (Li et al., 2014; Babaei and Joekar-Niasar, 2016; An et al., 2020b). The simplified assumption of perfect mixing, while computationally efficient, can lead to considerable errors at high Pe. In addition, the shearing of solute species inside pore throats, which occurs due to the parabolic profile of velocity streamlines, is also excluded from MCM (Mehmani and Balhoff, 2015a). Although the Taylor-Aris dispersion coefficient can partially address shear dispersion in pore throats, its effectiveness is limited due to the small length of throats (Mehmani and Tchelepi, 2017). A notable improvement to the perfect mixing assumption underlining MCM is the Streamline Splitting Method (SSM), using a sub-pore scale description for transport, representing pore bodies as made of multiple "pockets" of different concentration values which are affected by the number of inlets

into each pore (Mehmani et al., 2014).

4.2. Heterogeneity across scales

4.2.1. Field scale applications (large domains)

Structural heterogeneity across scales is an intrinsic feature of geological porous media, which can lead to scale-dependent, macroscopic (averaged) properties e.g. permeability or residence times (Liu et al., 2015; Muljadi et al., 2016; Aminnaji et al., 2019). The brute force approach of representing pore-scale processes in very large domains (e.g. field scale) is prohibitive by computational resources (Lunati and Jenny, 2006). However, continuum (averaged) models, even with selective grid refinement (Scheibe et al., 2015a), may still overlook crucial pore-scale details and thus result in considerable errors. Up-scaling, the "holy grail" of fluid dynamics in general and flow in porous media in particular, remains an open challenge (Li et al., 2006; Mehmani and Balhoff, 2015b; Yang et al., 2021b).

The aforementioned multiscale models offer a promising resolution by solving the flow and transport equations using different methods and spatial resolution.

4.2.2. Non-fickian transport

The Advection-DIspersion Equation (ADIE) describes solute transport at the Darcy scale. It captures well the transport when the solute spreads for a sufficiently long time and over a sufficiently large space compared to that of the flow inhomogeneities (Padilla et al., 1999; Neuman and Tartakovsky, 2009), such that it samples the entire velocity field and the transport asymptotically reaches the so-called Fickian regime (and concentration along the flow follows a Gaussian distribution) (Puyguiraud et al., 2021). Conversely, the ADIE fails to describe transport (e.g. dispersion and breakthrough) when the solute spreading exhibits a non-Gaussian breakthrough curve with long tails, a phenomenon denoted as non-Fickian or anomalous transport (Berkowitz et al., 2000; Cortis and Berkowitz, 2004; Zhang and Benson, 2008). Non-Fickian transport is promoted by spatial heterogeneity, as well as time-dependent velocity fields (Nissan et al., 2017; Nissan and Berkowitz, 2019). It is also enhanced by partial saturation: at given medium properties for which saturated transport is Fickian, reduction of the saturation can lead to strongly non-Fickian regimes, due to the development of highly non-uniform velocity fields and diffusion-controlled mass exchange between high- and low-velocity fields, termed mobile (or flowing) and immobile (trapped) (Guillon et al., 2013; Jimenez-Martinez et al., 2020; Velásquez-Parra et al., 2022). Fig. 4 displays solute migration at saturated (Fig. 4a) and unsaturated (Fig. 4b) conditions for a correlated porous medium.

Fluid-fluid boundaries create regions of high- and low-velocity fields, limiting the available pathways for solute solution. This leads to an early breakthrough time (compared to the saturated case) with non-Fickian tailing behavior (Fig. 4c).

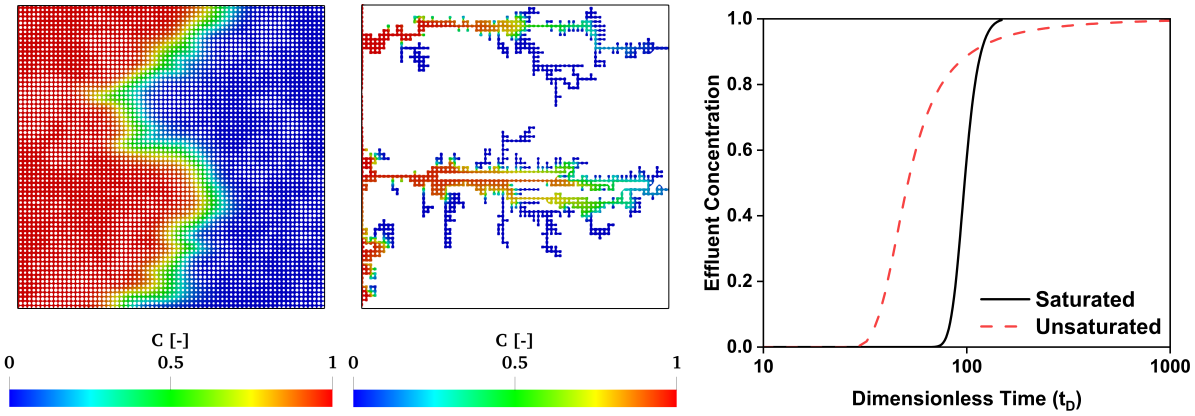

(a) (b) (c)

Figure 4: Solute transport at single and multiphase conditions in a porous medium with spatially-correlated pore sizes, simulated with OpenFOAM using VOF for capturing the fluid-fluid boundaries. Solute concentrations for the saturated case (a) at $t_D = 50$ and for the unsaturated case (b) at $t_D = 37$ show a marked difference: in the latter (b), the existence of flowing and trapped regions is evident. These differences are manifested in breakthrough curves (c), with long tails and early arrival time in the unsaturated case. Note that in (b) regions with no concentrations (white) are either solid phase or non-carrier fluid.

Anomalous spreading can be sub- or super-dispersive, that is slower or faster than predicted by Fick's law, respectively. These regimes are characterized by a power-law scaling of concentration variance, $\sigma^2 \sim t^\alpha$, where α (unity for Fickian) is smaller or greater than unity for sub- and super-dispersive, respectively (Zhang et al., 2012; Guillon et al., 2014). Super-dispersive transport is more common in highly heterogeneous domains such as fractured media and is mostly controlled by the preferential pathways with high-velocity fields. Different causes have been suggested for the sub-dispersive behavior, including mass transfer between low- and high-velocity zones or adsorption/desorption of the tracer by the solid phase (Guo et al., 2021).

Various methods were designed to capture anomalous and scale-dependent transport, using history-dependent transport equations with temporal and spatial nonlocality. Examples include Continuous Time Random Walk (CTRW) (Berkowitz et al., 2006; Noetinger et al., 2016; Kutner and Masoliver, 2017), Multi Rate Mass Transfer (MRMT) (Haggerty et al., 2000; Tecklenburg et al., 2016; Guo et al., 2020b), and Fractional ADIE (FADIE) (Zhang et al., 2009; Garrard et al., 2017; Qiao et al., 2020). These methods use a continuum statistical description which is not pore-scale

modeling and therefore are not discussed further here; for further details see e.g. Neuman and Tartakovsky (2009); Lu et al. (2018); Guo et al. (2021).

4.3. Impact of fluid displacement on solute transport

4.3.1. Dispersion and mixing vs. saturation

Dispersion vs. saturation. Contrasting results were found regarding the effect of saturation on the dispersion coefficient, making it a controversial, open topic. While some studies found an inverse relationship between dispersivity and carrier phase saturation (Padilla et al., 1999; Nützmann et al., 2002; Sato et al., 2003), others showed the opposite in undisturbed soils (increasing dispersion with saturation) (Hammel and Roth, 1998; Vanderborght and Vereecken, 2007). A potential explanation for the inverse relationship is that lower saturation amplifies preferential pathways, which in turn enhance spreading and dispersion. The opposite effect was explained by the positive correlation between the relative permeability and flow rate of the carrier fluid, directing flow to bigger pores. There were also observations of a non-monotonic relationship between dispersion and saturation (Birkholzer and Tsang, 1997; Raoof and Hassanizadeh, 2013; Karadimitriou et al., 2016, 2017; Gong and Piri, 2020; Zhuang et al., 2021; Dou et al., 2022), linking flow non-uniformity (impacted by variation in saturation) and dispersion coefficient.

Mixing vs. saturation. Mixing, affected by diffusion and local spreading (dispersion) in a relatively homogeneous medium, is also controlled by the stretching and folding of fluid elements associated with the complex structure of the medium (and hence velocity) in more heterogeneous media (Dentz et al., 2011; Heyman et al., 2020). An elaborated description of mixing is beyond the scope of this review, and interested readers can refer to a dedicated review study by Dentz et al. (2022). It is worth noting, however, that the distinction between mixing and dispersion is nontrivial (Le Borgne et al., 2015) and that even when spreading is Fickian mixing can become non-Fickian (Le Borgne et al., 2010; Boon et al., 2017).

Partial saturation has an intricate effect on mixing (Markale et al., 2021). Decreasing saturation typically increases the heterogeneity of velocity fields, promoting preferential pathways with shorter residence times for solute particles that reduce mixing (Ursino et al., 2001; Kapetas et al., 2014). However, preferential flow can promote concentration gradients between different regions, enhancing diffusive mass flux and thus mixing (Jimenez-Martinez et al., 2015, 2017). Jimenez-Martinez et al. (2015) concluded that there could be different mechanisms that affect mixing at unsaturated porous media: (1) development of preferential flow pathways that create low- and high-velocity zones; (2)

non-Fickian behavior that sustains concentration gradients; and (3) coalescence of pathways due to the presence of very high-velocity spots. Other studies also highlighted the decisive role of the mass exchange rate between flowing and trapped regions and its dependence on concentration gradients, the geometry of the pores, and, in particular, the interfaces between these regions (Haggerty et al., 2004; Karadimitriou et al., 2016; Aziz et al., 2018; Hasan et al., 2019; An et al., 2020b).

4.3.2. Three-dimensional effects

A quasi-2D domain in the form of a thin gap (of a much smaller length than the dimensions in the perpendicular plane) is widely used both experimentally and computationally. Beyond simplifying design, measurement, and visualization in experiments and reducing computational complexity and run-time, reducing the dimensionality also can simplify the physics and thus allow more fundamental understanding e.g. of the effect of pore structure. The confinement of flow in the third dimension can significantly impact the flow field and interface configuration, especially when the thickness is comparable to the pore apertures (Chen et al., 2018b). To account for this effect in a 2D model without resolving the full 3D pore geometry, an additional Darcy-like term was introduced to the NS momentum equation (Horgue et al., 2013; Ferrari et al., 2015),

$$\frac{\partial \rho \mathbf{u}}{\partial t} + \nabla.(\rho \mathbf{u}\mathbf{u}) = -\nabla P + \nabla.(\mu(\nabla \mathbf{u} + \nabla \mathbf{u}^T)) + \rho \mathbf{g} + \mathbf{F_s} - \mathbf{u}\frac{\mu}{k} \tag{30}$$

The permeability in Eq. 30 is expressed as a function of the gap thickness b, as $k = b^2/12$. The interface curvature at a local point is the sum of curvatures in the direction of flow (κ_{xy}) and perpendicular to it (κ_z). Assuming capillary equilibrium, the interface curvature is determined by

$$\kappa = -\nabla \cdot \mathbf{n} - \frac{2}{b}\cos\theta \tag{31}$$

where θ is the contact angle of the interface to the solid boundary.

4.3.3. Wettability effects

One of the biggest challenges in modeling fluid displacement is representing the surface forces associated with the wetting of the solid by the fluids. Methodologies describing wettability include lubrication theory, pairwise interaction forces, and contact angle (Huber et al., 2016; Guo et al., 2020a). In capillary-controlled displacement, a thin film can be deposited on the solid wall, prohibiting direct contact of the non-wetting phase with the solid. The sub-pore scale dimension of the film makes accurate modeling of its evolution computationally prohibitive. The lubrication approximation is a sub-pore scale model that solves a nonlinear partial differential equation for the

film evolution (Roman et al., 2017), which has been also incorporated in a multi-phase flow model (Qin et al., 2020).

The most common description of wettability is via the contact angle between the fluids and the surface. Most studies of porous media consider a static (equilibrium) contact angle, namely identical advancing and receding contact angles, ignoring the effect of hysteresis related to the direction of advancement or flow velocity (dynamics) (Rabbani et al., 2017; Friis et al., 2019; Rabbani and Seers, 2019; Ambekar et al., 2021b; Jettestuen et al., 2021; Yang et al., 2021c), in contrast with the more picture exposed by experimental and theoretical studies showing different advancing and receding contact angles (Lam et al., 2002; Chibowski, 2007) as well as contact angle variations in both space (due to the surface roughness and chemistry) (Alhammadi et al., 2017; AlRatrout et al., 2017; Nazari et al., 2022) and time (Bandara et al., 2016). Neglecting these aspects can lead to discrepancies in the predicted displacement patterns (Tembely et al., 2020).

4.3.4. Sensitivity to phase distribution

To exemplify the appreciable effect of uncertainty in interface configuration and the resulting fluid velocity fields on solute transport, we compare simulations in four idealized media of identical pore geometry which vary by a single pore occupancy (e.g. resulting from snap off), corresponding to a minute variation in phase saturation (less than 0.3%), cf. Fig. S1 in Supplementary Material (SM), Fig. 5a shows pattern C. Simulations (run in OpenFoam) of pulse injection were conducted for the four patterns at $Pe = 80$ (see numerical details in SM). While the removed pores' occupancy hardly affected saturation, their effect on phase connectivity was significant. This, in turn, strongly affected the tortuosity of streamlines and solute solution dispersivity. Consequently, the (macroscopic) breakthrough curves show a striking $\sim$20% increase in the peak concentration (Fig. 5b), and longer tails of high concentration in the less-connected patterns (Fig. 5c), indicating a progressively more non-Fickian behavior caused by gradual washout of the solute from the medium. The non-Fickian behavior reflects the mass exchange between high- and low-velocity regions, which happens primarily by diffusive mass flux. This remarkable difference in transport can be explained quantitatively via the contributions of different regions, comparing the probability distribution of pore velocities (or equivalent pore-scale Peclet number, see SM). This reveals the emergence of a low velocity, diffusion-controlled ("dead-end") region.

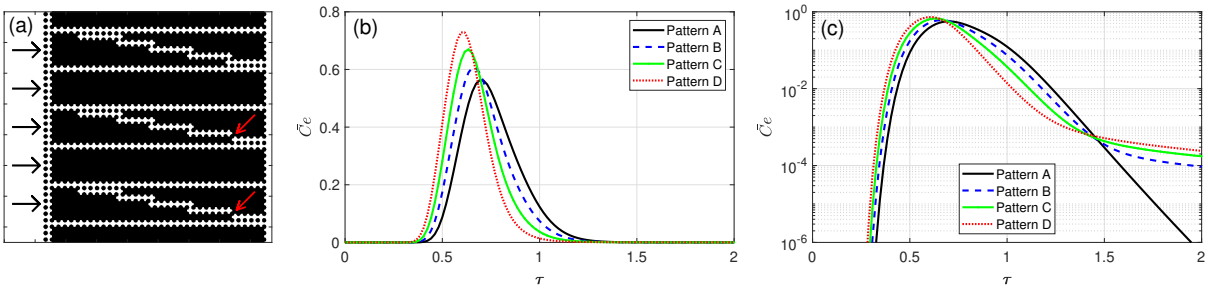

Figure 5: Sensitivity of solute transport to uncertainty in multiphase fluid displacement is demonstrated by comparing transport in four almost identical patterns of the carrier phase. The four patterns, consisting of 6 straight and 3 diagonal channels, differ by a single pore occupancy; in pattern A, all channels are clear, in pattern B, one diagonal channel is obstructed, in pattern C, two diagonal channels are obstructed (shown in Panel (a) with red arrows), and in pattern D, only straight channels are clear. The flow direction is from left to right (black arrows). Solute breakthrough curves at the outlet are shown in linear (b) and logarithmic (c) scales. We use dimensionless time $\tau = t\ V_0/L\phi$, where t is time, V_0 is the inlet velocity, L is the domain length, and ϕ is porosity. Blockage of pathways, which causes dead-end regions, is shown to increase the concentration peak (b) and the concentration tails (c), exhibiting non-Fickian behavior due to the solute washout from stagnant areas; observe the well-defined exponential tail in pattern A.

5. Concluding remarks

Advancements in pore-scale modeling techniques have improved our understanding of how solutes migrate in partially-saturated porous media. Nonetheless, several pervasive challenges remain, including nonphysical ("spurious") fluxes, and representation of boundaries or interfaces and the interfacial forces acting there, in particular wetting. These challenges in simulating multiphase flow are shown here to have a meaningful impact on the prediction of solute transport in unsaturated conditions.

The choice of pore-scale modeling method depends on the required resolution and the trade-off between accuracy and computational cost, which can vary among applications. Highly resolved, direct approaches (CFD) provide a reasonably accurate pore-scale description of the flow field. However, even with the rapidly increasing computational power, simulations of a sufficiently large domain to capture multiscale heterogeneity are expected to remain prohibitive, in particular, in geosciences where such heterogeneity is inherent. PNM offers a substantially increased computational efficiency, allowing up-scaling to sample and possibly to the field scale. However, this is achieved at the expense of overly simplified pore geometries and pore-level mixing. Multiscale models are a promising compromise between the scale of simulated domains, the level of details in regions where they matter the most, and thus computational cost. Finally, further improvement of

techniques requires validation against both pore-scale experiments (Datta et al., 2023)) as well as the larger, macroscopic scales from the laboratory (Flemisch et al., 2023) to the field (Dentz et al., 2020) scales.

Acknowledgments

RH acknowledges support from the Engineering and Physical Sciences Research Council (EP/V050613/1). SA was supported by the SMEP Programme funded by FCDO (IATI reference number GB-GOV-1–30012). The authors acknowledge resources and support from Coventry University HPC facilities and the Scientific Computing RTP at the University of Warwick.

References

Acharya, R., Van der Zee, S., Leijnse, A., 2007. Approaches for modeling longitudinal dispersion in pore-networks. Adv. Water Resour. 30, 261–272. doi:10.1016/j.advwatres.2005.11.015.

Afshari, S., Hejazi, S.H., Kantzas, A., 2018. Longitudinal dispersion in heterogeneous layered porous media during stable and unstable pore-scale miscible displacements. Adv. Water Resour. 119, 125–141. doi:10.1016/j.advwatres.2018.06.005.

Aghaei, A., Piri, M., 2015. Direct pore-to-core up-scaling of displacement processes: Dynamic pore network modeling and experimentation. J. Hydrol. 522, 488–509. doi:10.1016/j.jhydrol.2015.01.004.

Akai, T., Bijeljic, B., Blunt, M.J., 2018. Wetting boundary condition for the color-gradient lattice Boltzmann method: Validation with analytical and experimental data. Adv. Water Resour. 116, 56–66. doi:10.1016/j.advwatres.2018.03.014.

Akai, T., Blunt, M.J., Bijeljic, B., 2020. Pore-scale numerical simulation of low salinity water flooding using the lattice Boltzmann method. J. Colloid Interface Sci. 566, 444–453. doi:10.1016/j.jcis.2020.01.065.

Aker, E., Måløy, K.J., Hansen, A., 1998. Simulating temporal evolution of pressure in two-phase flow in porous media. Phys. Rev. E 58, 2217–2226. doi:10.1103/PhysRevE.58.2217.

Albadawi, A., Donoghue, D., Robinson, A., Murray, D., Delauré, Y., 2013. Influence of surface tension implementation in volume of fluid and coupled volume of fluid with

level set methods for bubble growth and detachment. Int. J. Multiph. Flow 53, 11–28. doi:10.1016/j.ijmultiphaseflow.2013.01.005.

Alhammadi, A.M., AlRatrout, A., Singh, K., Bijeljic, B., Blunt, M.J., 2017. In situ characterization of mixed-wettability in a reservoir rock at subsurface conditions. Sci. Rep. 7, 10753. doi:10.1038/s41598-017-10992-w.

AlRatrout, A., Raeini, A.Q., Bijeljic, B., Blunt, M.J., 2017. Automatic measurement of contact angle in pore-space images. Adv. Water Resour. 109, 158–169. doi:10.1016/j.advwatres.2017.07.018.

Ambekar, A.S., Mattey, P., Buwa, V.V., 2021a. Pore-resolved two-phase flow in a pseudo-3D porous medium: Measurements and volume-of-fluid simulations. Chem. Eng. Sci. 230, 116128. doi:10.1016/j.ces.2020.116128.

Ambekar, A.S., Mondal, S., Buwa, V.V., 2021b. Pore-resolved volume-of-fluid simulations of two-phase flow in porous media: Pore-scale flow mechanisms and regime map. Phys. Fluids 33, 102119. doi:10.1063/5.0064833.

Aminnaji, M., Rabbani, A., J. Niasar, V., Babaei, M., 2019. Effects of pore-scale heterogeneity on macroscopic napl dissolution efficiency: A two-scale numerical simulation study. Water Resour. Res. 55, 8779–8799. doi:10.1029/2019WR026035.

An, S., Erfani, H., Godinez-Brizuela, O.E., Niasar, V., 2020a. Transition from viscous fingering to capillary fingering: Application of gpu-based fully implicit dynamic pore network modeling. Water Resour. Res. 56, e2020WR028149. doi:10.1029/2020WR028149.

An, S., Hasan, S., Erfani, H., Babaei, M., Niasar, V., 2020b. Unravelling effects of the pore-size correlation length on the two-phase flow and solute transport properties: Gpu-based pore-network modeling. Water Resour. Res. 56, e2020WR027403. doi:10.1029/2020WR027403.

Armstrong, R.T., Sun, C., Mostaghimi, P., Berg, S., Rücker, M., Luckham, P., Georgiadis, A., McClure, J.E., 2021. Multiscale characterization of wettability in porous media. Transp. Porous Media 140, 215–240. doi:10.1007/s11242-021-01615-0.

Aziz, R., Joekar-Niasar, V., Martinez-Ferrer, P., 2018. Pore-scale insights into transport and mixing in steady-state two-phase flow in porous media. Int. J. Multiph. Flow 109, 51–62. doi:10.1016/j.ijmultiphaseflow.2018.07.006.

769 Aziz, R., Joekar-Niasar, V., Martinez-Ferrer, P.J., Godinez-Brizuela, O.E., Theodoropoulos, C.,
770 Mahani, H., 2019. Novel insights into pore-scale dynamics of wettability alteration during low
771 salinity waterflooding. Sci. Rep. 9, 1–13.

772 Aziz, R., Niasar, V., Erfani, H., Martinez-Ferrer, P.J., 2020. Impact of pore mor-
773 phology on two-phase flow dynamics under wettability alteration. Fuel 268, 117315.
774 doi:10.1016/j.fuel.2020.117315.

775 Babaei, M., Joekar-Niasar, V., 2016. A transport phase diagram for pore-level correlated porous
776 media. Adv. Water Resour. 92, 23–29. doi:10.1016/j.advwatres.2016.03.014.

777 Bakhshian, S., Hosseini, S.A., 2019. Pore–scale analysis of supercritical CO2–brine immisci-
778 ble displacement under fractional–wettability conditions. Adv. Water Resour. 126, 96–107.
779 doi:10.1016/j.advwatres.2019.02.008.

780 Bandara, U.C., Palmer, B.J., Tartakovsky, A.M., 2016. Effect of wettability alteration on long-term
781 behavior of fluids in subsurface. Comput. Part. Mech. 3, 277–289. doi:10.1007/s40571-015-0098-8.

782 Ben-Noah, I., Hidalgo, J.J., Jimenez-Martinez, J., Dentz, M., 2023. Solute trapping and the
783 mechanisms of non-fickian transport in partially saturated porous media. Water Resour. Res.
784 59, e2022WR033613. doi:10.1029/2022WR033613.

785 Berkowitz, B., Cortis, A., Dentz, M., Scher, H., 2006. Modeling non-fickian transport in geological
786 formations as a continuous time random walk. Rev. Geophys. 44. doi:10.1029/2005RG000178.

787 Berkowitz, B., Scher, H., Silliman, S.E., 2000. Anomalous transport in laboratory-scale, heteroge-
788 neous porous media. Water Resour. Res. 36, 149–158. doi:10.1029/1999WR900295.

789 Bhattad, P., Willson, C.S., Thompson, K.E., 2011. Effect of network structure on characterization
790 and flow modeling using x-ray micro-tomography images of granular and fibrous porous media.
791 Transp. Porous Media 90, 363–391.

792 Bijeljic, B., Blunt, M.J., 2006. Pore-scale modeling and continuous time random walk analysis of
793 dispersion in porous media. Water Resour. Res. 42.

794 Bijeljic, B., Blunt, M.J., 2007. Pore-scale modeling of transverse dispersion in porous media. Water
795 Resour. Res. 43.

Bilger, C., Aboukhedr, M., Vogiatzaki, K., Cant, R.S., 2017. Evaluation of two-phase flow solvers using level set and volume of fluid methods. J. Comput. Phys. 345, 665–686. doi:10.1016/j.jcp.2017.05.044.

Birkholzer, J., Tsang, C.F., 1997. Solute channeling in unsaturated heterogeneous porous media. Water Resour. Res. 33, 2221–2238.

Biswas, S., Fantinel, P., Borgman, O., Holtzman, R., Goehring, L., 2018. Drying and percolation in correlated porous media. Phys. Rev. Fluids 3, 124307.

Blunt, M.J., 2001. Flow in porous media—pore-network models and multiphase flow. Curr. Opin. Colloid. Interface 6, 197–207.

Blunt, M.J., 2017. Multiphase Flow in Permeable Media: A Pore-Scale Perspective. Cambridge University Press, Cambridge. doi:10.1017/9781316145098.

Blunt, M.J., Bijeljic, B., Dong, H., Gharbi, O., Iglauer, S., Mostaghimi, P., Paluszny, A., Pentland, C., 2013. Pore-scale imaging and modelling. Adv. Water Resour. 51, 197–216.

Bonto, M., Welch, M., Lüthje, M., Andersen, S., Veshareh, M., Amour, F., Afrough, A., Mokhtari, R., Hajiabadi, M., Alizadeh, M., et al., 2021. Challenges and enablers for large-scale CO2 storage in chalk formations. Earth Sci. Rev. 222, 103826.

Boon, M., Bijeljic, B., Krevor, S., 2017. Observations of the impact of rock heterogeneity on solute spreading and mixing. Water Resour. Res. 53, 4624–4642.

Borgman, O., Darwent, T., Segre, E., Goehring, L., Holtzman, R., 2019. Immiscible fluid displacement in porous media with spatially correlated particle sizes. Adv. Water Resour. 128, 158–167. doi:10.1016/j.advwatres.2019.04.015.

Borgman, O., Turuban, R., Géraud, B., Le Borgne, T., Méheust, Y., 2023. Solute front shear and coalescence control concentration gradient dynamics in porous micromodel. Geophys. Res. Lett. 50, e2022GL101407.

Brackbill, J.U., Kothe, D.B., Zemach, C., 1992. A continuum method for modeling surface tension. J. Comput. Phys. 100, 335–354. doi:10.1016/0021-9991(92)90240-Y.

Brinkman, H.C., 1949. A calculation of the viscous force exerted by a flowing fluid on a dense swarm of particles. Flow, Turbulence and Combustion 1, 27–34.

824 Bui, H.H., Nguyen, G.D., 2021. Smoothed particle hydrodynamics (SPH) and its applications in
825 geomechanics: From solid fracture to granular behaviour and multiphase flows in porous media.
826 Comput. Geotech. 138, 104315.

827 Bultreys, T., De Boever, W., Cnudde, V., 2016. Imaging and image-based fluid transport modeling
828 at the pore scale in geological materials: A practical introduction to the current state-of-the-art.
829 Earth Sci. Rev. 155, 93–128.

830 Bultreys, T., Lin, Q., Gao, Y., Raeini, A.Q., AlRatrout, A., Bijeljic, B., Blunt, M.J., 2018. Val-
831 idation of model predictions of pore-scale fluid distributions during two-phase flow. Phys. Rev.
832 E 97, 053104.

833 Bultreys, T., Van Hoorebeke, L., Cnudde, V., 2015. Multi-scale, micro-computed tomography-
834 based pore network models to simulate drainage in heterogeneous rocks. Adv. Water Resour. 78,
835 36–49.

836 Cao, Z., Zhou, J., Liu, A., Sun, D., Yu, B., Wei, J., 2020. A three dimensional coupled VOF and
837 Level Set (VOSET) method with and without phase change on general curvilinear grids. Chem.
838 Eng. Sci. 223, 115705. doi:10.1016/j.ces.2020.115705.

839 Chen, L., He, A., Zhao, J., Kang, Q., Li, Z.Y., Carmeliet, J., Shikazono, N., Tao, W.Q., 2022.
840 Pore-scale modeling of complex transport phenomena in porous media. Prog. Energy Combust.
841 Sci. 88, 100968.

842 Chen, L., Kang, Q., Mu, Y., He, Y.L., Tao, W.Q., 2014. A critical review of the pseudopotential
843 multiphase lattice Boltzmann model: Methods and applications. Int. J. Heat Mass Transf. 76,
844 210–236. doi:10.1016/j.ijheatmasstransfer.2014.04.032.

845 Chen, L., Kang, Q., Robinson, B.A., He, Y.L., Tao, W.Q., 2013. Pore-scale modeling of multi-
846 phase reactive transport with phase transitions and dissolution-precipitation processes in closed
847 systems. Phys. Rev. E 87, 043306.

848 Chen, L., Luan, H.B., He, Y.L., Tao, W.Q., 2012. Pore-scale flow and mass transport in gas diffusion
849 layer of proton exchange membrane fuel cell with interdigitated flow fields. Int. J. Therm. Sci.
850 51, 132–144.

Chen, L., Zhang, R., Min, T., Kang, Q., Tao, W., 2018a. Pore-scale study of effects of macroscopic pores and their distributions on reactive transport in hierarchical porous media. J. Chem. Eng. 349, 428–437.

Chen, Y., Li, Y., Valocchi, A.J., Christensen, K.T., 2018b. Lattice Boltzmann simulations of liquid CO2 displacing water in a 2D heterogeneous micromodel at reservoir pressure conditions. J. Contam. Hydrol. 212, 14–27.

Chen, Y., Valocchi, A.J., Kang, Q., Viswanathan, H.S., 2019. Inertial effects during the process of supercritical CO2 displacing brine in a sandstone: Lattice Boltzmann simulations based on the continuum-surface-force and geometrical wetting models. Water Resour. Res. 55, 11144–11165.

Chibowski, E., 2007. On some relations between advancing, receding and Young's contact angles. Adv. Colloid Interface Sci. 133, 51–59. doi:10.1016/j.cis.2007.03.002.

Corada-Fernández, C., Jiménez-Martínez, J., Candela, L., González-Mazo, E., Lara-Martín, P.A., 2015. Occurrence and spatial distribution of emerging contaminants in the unsaturated zone. case study: Guadalete river basin (cadiz, spain). Chemosphere 119, S131–S137.

Coreixas, C., Chopard, B., Latt, J., 2019. Comprehensive comparison of collision models in the lattice Boltzmann framework: Theoretical investigations. Phys. Rev. E 100, 033305. doi:10.1103/PhysRevE.100.033305.

Cortis, A., Berkowitz, B., 2004. Anomalous transport in "classical" soil and sand columns. Soil Sci. Soc. Am. J. 68, 1539–1548.

Datta, S.S., Battiato, I., Fernø, M.A., Juanes, R., Parsa, S., Prigiobbe, V., Santanach-Carreras, E., Song, W., Biswal, S.L., Sinton, D., 2023. Lab chip for a low-carbon future. Lab Chip 23, 1358–1375.

De Anna, P., Dentz, M., Tartakovsky, A., Le Borgne, T., 2014. The filamentary structure of mixing fronts and its control on reaction kinetics in porous media flows. Geophys. Res. Lett. 41, 4586–4593.

De Gennes, P., 1983. Hydrodynamic dispersion in unsaturated porous media. J. Fluid Mech. 136, 189–200.

878 Dehshibi, R.R., Sadatshojaie, A., Mohebbi, A., Riazi, M., 2019. A new insight into pore body filling
879 mechanism during waterflooding in a glass micro-model. Chem. Eng. Res. Des. 151, 100–107.

880 Deng, H., Gharasoo, M., Zhang, L., Dai, Z., Hajizadeh, A., Peters, C.A., Soulaine, C., Thullner,
881 M., Van Cappellen, P., 2022. A perspective on applied geochemistry in porous media: Reactive
882 transport modeling of geochemical dynamics and the interplay with flow phenomena and physical
883 alteration. Applied Geochemistry , 105445.

884 Dentz, M., Comolli, A., Hakoun, V., Hidalgo, J.J., 2020. Transport upscaling in highly heteroge-
885 neous aquifers and the prediction of tracer dispersion at the made site. Geophys. Res. Lett. 47,
886 e2020GL088292.

887 Dentz, M., Hidalgo, J.J., Lester, D., 2022. Mixing in porous media: Concepts and approaches
888 across scales. Transp. Porous Media , 1–49.

889 Dentz, M., Le Borgne, T., Englert, A., Bijeljic, B., 2011. Mixing, spreading and reaction in
890 heterogeneous media: A brief review. J. Contam. Hydrol. 120, 1–17.

891 Dianat, M., Skarysz, M., Garmory, A., 2017. A coupled level set and volume of fluid method for
892 automotive exterior water management applications. Int. J. Multiph. Flow 91, 19–38.

893 Dou, Z., Zhang, X., Zhuang, C., Yang, Y., Wang, J., Zhou, Z., 2022. Saturation dependence of
894 mass transfer for solute transport through residual unsaturated porous media. Int. J. Heat Mass
895 Transf. 188, 122595.

896 Erfani, H., Karadimitriou, N., Nissan, A., Walczak, M.S., An, S., Berkowitz, B., Niasar, V., 2021.
897 Process-dependent solute transp. porous media. Transp. Porous Media 140, 421–435.

898 Fan, M., Dalton, L.E., McClure, J., Ripepi, N., Westman, E., Crandall, D., Chen, C., 2019.
899 Comprehensive study of the interactions between the critical dimensionless numbers associated
900 with multiphase flow in 3D porous media. Fuel 252, 522–533.

901 Fatt, I., 1956. The network model of porous media. Transactions of the AIME 207, 144–181.
902 doi:10.2118/574-g.

903 Federico, I., Marrone, S., Colagrossi, A., Aristodemo, F., Antuono, M., 2012. Simulating 2D
904 open-channel flows through an SPH model. Eur. J. Mech. B/Fluids 34, 35–46.

905 Ferrari, A., Jimenez-Martinez, J., Borgne, T.L., Méheust, Y., Lunati, I., 2015. Challenges in
906 modeling unstable two-phase flow experiments in porous micromodels. Water Resour. Res. 51,
907 1381–1400.

908 Flemisch, B., Nordbotten, J.M., Fernø, M., Juanes, R., Class, H., Delshad, M., Doster, F., Ennis-
909 King, J., Franc, J., Geiger, S., et al., 2023. The fluidflower international benchmark study:
910 Process, modeling results, and comparison to experimental data. arXiv:2302.10986[physics.geo-
911 ph] .

912 Francois, M.M., Cummins, S.J., Dendy, E.D., Kothe, D.B., Sicilian, J.M., Williams, M.W., 2006.
913 A balanced-force algorithm for continuous and sharp interfacial surface tension models within a
914 volume tracking framework. J. Comput. Phys. 213, 141–173.

915 Friis, H.A., Pedersen, J., Jettestuen, E., Helland, J.O., Prodanovic, M., 2019. Pore-scale level set
916 simulations of capillary-controlled displacement with adaptive mesh refinement. Transp. Porous
917 Media 128, 123–151. doi:10.1007/s11242-019-01238-6.

918 Garrard, R.M., Zhang, Y., Wei, S., Sun, H., Qian, J., 2017. Can a time fractional-derivative model
919 capture scale-dependent dispersion in saturated soils? Groundwater 55, 857–870.

920 Golparvar, A., Zhou, Y., Wu, K., Ma, J., Yu, Z., 2018. A comprehensive review of pore scale
921 modeling methodologies for multiphase flow in porous media. Adv. Geo-Energy Res. 2, 418–440.

922 Gong, Y., Piri, M., 2020. Pore-to-core upscaling of solute transport under steady-state two-phase
923 flow conditions using dynamic pore network modeling approach. Transp. Porous Media 135,
924 181–218.

925 Gopala, V.R., van Wachem, B.G., 2008. Volume of fluid methods for immiscible-fluid and free-
926 surface flows. J. Chem. Eng. 141, 204–221.

927 Guédon, G.R., Inzoli, F., Riva, M., Guadagnini, A., 2019. Pore-scale velocities in three-dimensional
928 porous materials with trapped immiscible fluid. Phys. Rev. E 100, 043101.

929 Guillon, V., Bauer, D., Fleury, M., Néel, M.C., 2014. Computing the longtime behaviour of nmr
930 propagators in porous media using a pore network random walk model. Transp. Porous Media
931 101, 251–267.

Guillon, V., Fleury, M., Bauer, D., Neel, M.C., 2013. Superdispersion in homogeneous unsaturated porous media using nmr propagators. Phys. Rev. E 87, 043007.

Gunstensen, A.K., Rothman, D.H., Zaleski, S., Zanetti, G., 1991. Lattice Boltzmann model of immiscible fluids. Phys. Rev. A 43, 4320.

Guo, H., Nazari, N., Esmaeilzadeh, S., Kovscek, A.R., 2020a. A critical review of the role of thin liquid films for modified salinity brine recovery processes. Curr. Opin. Colloid. Interface 50, 101393.

Guo, Z., Henri, C.V., Fogg, G.E., Zhang, Y., Zheng, C., 2020b. Adaptive multirate mass transfer (ammt) model: A new approach to upscale regional-scale transport under transient flow conditions. Water Resour. Res. 56, e2019WR026000.

Guo, Z., Ma, R., Zhang, Y., Zheng, C., 2021. Contaminant transport in heterogeneous aquifers: A critical review of mechanisms and numerical methods of non-fickian dispersion. Science China Earth Sciences 64, 1224–1241.

Haggerty, R., Harvey, C.F., Freiherr von Schwerin, C., Meigs, L.C., 2004. What controls the apparent timescale of solute mass transfer in aquifers and soils? a comparison of experimental results. Water Resour. Res. 40.

Haggerty, R., McKenna, S.A., Meigs, L.C., 2000. On the late-time behavior of tracer test breakthrough curves. Water Resour. Res. 36, 3467–3479.

Haghshenas, M., Wilson, J.A., Kumar, R., 2017. Algebraic coupled level set-volume of fluid method for surface tension dominant two-phase flows. Int. J. Multiph. Flow 90, 13–28. doi:10.1016/j.ijmultiphaseflow.2016.12.002.

Hammel, K., Roth, K., 1998. Approximation of asymptotic dispersivity of conservative solute in unsaturated heterogeneous media with steady state flow. Water Resour. Res. 34, 709–715.

Hasan, S., Joekar-Niasar, V., Karadimitriou, N.K., Sahimi, M., 2019. Saturation dependence of non-fickian transp. porous media. Water Resour. Res. 55, 1153–1166.

Hasan, S., Niasar, V., Karadimitriou, N.K., Godinho, J.R., Vo, N.T., An, S., Rabbani, A., Steeb, H., 2020. Direct characterization of solute transport in unsaturated porous media using fast x-ray synchrotron microtomography. Proc. Natl. Acad. Sci. 117, 23443–23449.

He, Y.L., Liu, Q., Li, Q., Tao, W.Q., 2019. Lattice Boltzmann methods for single-phase and solid-liquid phase-change heat transfer in porous media: A review. Int. J. Heat Mass Transf. 129, 160–197.

Heyman, J., Lester, D.R., Turuban, R., Méheust, Y., Le Borgne, T., 2020. Stretching and folding sustain microscale chemical gradients in porous media. Proc. Natl. Acad. Sci. 117, 13359–13365.

Hirschler, M., Oger, G., Nieken, U., Le Touze, D., 2017. Modeling of droplet collisions using smoothed particle hydrodynamics. Int. J. Multiph. Flow 95, 175–187. doi:10.1016/j.ijmultiphaseflow.2017.06.002.

Hoang, D.A., van Steijn, V., Portela, L.M., Kreutzer, M.T., Kleijn, C.R., 2013. Benchmark numerical simulations of segmented two-phase flows in microchannels using the volume of fluid method. Comput. Fluids 86, 28–36.

Holmes, D.W., Pivonka, P., 2021. Novel pressure inlet and outlet boundary conditions for smoothed particle hydrodynamics, applied to real problems in porous media flow. J. Comput. Phys. 429, 110029.

Holmes, D.W., Williams, J.R., Tilke, P., 2011. Smooth particle hydrodynamics simulations of low reynolds number flows through porous media. Int. J. Numer. Anal. Methods Geomech. 35, 419–437.

Holtzman, R., 2016. Effects of pore-scale disorder on fluid displacement in partially-wettable porous media. Sci. Rep. 6, 36221. doi:10.1038/srep36221.

Holtzman, R., Juanes, R., 2010. Crossover from fingering to fracturing in deformable disordered media. Phys. Rev. E 82, 046305.

Horgue, P., Augier, F., Duru, P., Prat, M., Quintard, M., 2013. Experimental and numerical study of two-phase flows in arrays of cylinders. Chem. Eng. Sci. 102, 335–345.

Hosseini, S.M., Feng, J.J., 2011. Pressure boundary conditions for computing incompressible flows with SPH. J. Comput. Phys. 230, 7473–7487.

Hosseinzadegan, A., Raoof, A., Mahdiyar, H., Nikooee, E., Ghaedi, M., Qajar, J., 2023. Review on pore-network modeling studies of gas-condensate flow: Pore structure, mechanisms, and implementations. Geoenergy Sci. Eng. , 211693.

Hu, R., Wan, J., Kim, Y., Tokunaga, T.K., 2017. Wettability effects on supercritical CO2–brine immiscible displacement during drainage: Pore-scale observation and 3D simulation. Int. J. Greenh. Gas Control 60, 129–139. doi:10.1016/j.ijggc.2017.03.011.

Huang, H., Thorne Jr, D.T., Schaap, M.G., Sukop, M.C., 2007. Proposed approximation for contact angles in shan-and-chen-type multicomponent multiphase lattice Boltzmann models. Phys. Rev. E 76, 066701.

Huang, X., Bandilla, K.W., Celia, M.A., 2016. Multi-physics pore-network modeling of two-phase shale matrix flows. Transp. Porous Media 111, 123–141.

Huang, X., Zhou, W., Deng, D., 2020. Validation of pore network modeling for determination of two-phase transport in fibrous porous media. Sci. Rep. 10, 20852. doi:10.1038/s41598-020-74581-0.

Huber, M., Keller, F., Sackel, W., Hirschler, M., Kunz, P., Hassanizadeh, S.M., Nieken, U., 2016. On the physically based modeling of surface tension and moving contact lines with dynamic contact angles on the continuum scale. J. Comput. Phys. 310, 459–477. doi:10.1016/j.jcp.2016.01.030.

Huysmans, M., Dassargues, A., 2005. Review of the use of péclet numbers to determine the relative importance of advection and diffusion in low permeability environments. Hydrogeol. J. 13, 895–904.

Ikeda, M., Rao, P., Schaefer, L., 2014. A thermal multicomponent lattice Boltzmann model. Comput. Fluids 101, 250–262.

Jamshidi, F., Heimel, H., Hasert, M., Cai, X., Deutschmann, O., Marschall, H., Wörner, M., 2019. On suitability of phase-field and algebraic volume-of-fluid OpenFOAM® solvers for gas–liquid microfluidic applications. Comput. Phys. Commun. 236, 72–85.

Jettestuen, E., Friis, H.A., Helland, J.O., 2021. A locally conservative multiphase level set method for capillary-controlled displacements in porous media. J. Comput. Phys. 428, 109965. doi:10.1016/j.jcp.2020.109965.

Jiang, F., Oliveira, M.S., Sousa, A.C., 2007. Mesoscale SPH modeling of fluid flow in isotropic porous media. Comput. Phys. Commun. 176, 471–480.

Jiang, Z., Van Dijke, M., Sorbie, K.S., Couples, G.D., 2013. Representation of multiscale heterogeneity via multiscale pore networks. Water Resour. Res. 49, 5437–5449.

Jimenez-Martinez, J., Alcolea, A., Straubhaar, J.A., Renard, P., 2020. Impact of phases distribution on mixing and reactions in unsaturated porous media. Adv. Water Resour. 144, 103697.

Jimenez-Martinez, J., Anna, P.d., Tabuteau, H., Turuban, R., Borgne, T.L., Meheust, Y., 2015. Pore-scale mechanisms for the enhancement of mixing in unsaturated porous media and implications for chemical reactions. Geophys. Res. Lett. 42, 5316–5324.

Jimenez-Martinez, J., Le Borgne, T., Tabuteau, H., Meheust, Y., 2017. Impact of saturation on dispersion and mixing in porous media: Photobleaching pulse injection experiments and shear-enhanced mixing model. Water Resour. Res. 53, 1457–1472.

Joekar-Niasar, V., 2016. Pore-scale modelling techniques: balancing efficiency, performance, and robustness. Comput. Geosci. 20, 773.

Joekar-Niasar, V., Hassanizadeh, S.M., 2012. Analysis of fundamentals of two-phase flow in porous media using dynamic pore-network models: A review. Crit. Rev. Environ. Sci. Technol. 42, 1895–1976. doi:10.1080/10643389.2011.574101.

Juanes, R., Meng, Y., Primkulov, B.K., 2020. Multiphase flow and granular mechanics. Phys. Rev. Fluids 5, 110516. doi:10.1103/PhysRevFluids.5.110516.

Kang, S.K., Hassan, Y.A., 2013. The effect of lattice models within the lattice Boltzmann method in the simulation of wall-bounded turbulent flows. J. Comput. Phys. 232, 100–117.

Kapetas, L., Dror, I., Berkowitz, B., 2014. Evidence of preferential path formation and path memory effect during successive infiltration and drainage cycles in uniform sand columns. J. Contam. Hydrol. 165, 1–10.

Karadimitriou, N.K., Joekar-Niasar, V., Babaei, M., Shore, C.A., 2016. Critical role of the immobile zone in non-fickian two-phase transport: A new paradigm. Environ. Sci. Technol. 50, 4384–4392.

Karadimitriou, N.K., Joekar-Niasar, V., Brizuela, O.G., 2017. Hydro-dynamic solute transport under two-phase flow conditions. Sci. Rep. 7, 1–7.

Khayrat, K., Jenny, P., 2016. Subphase approach to model hysteretic two-phase flow in porous media. Transp. Porous Media 111, 1–25.

Kitanidis, P.K., 1994. The concept of the dilution index. Water Resour. Res. 30, 2011–2026.

Kulasiri, D., Verwoerd, W., 2002. Stochastic Dynamics. Modeling Solute Transp. Porous Media. Elsevier.

Kunz, P., Zarikos, I., Karadimitriou, N., Huber, M., Nieken, U., Hassanizadeh, S., 2016. Study of multi-phase flow in porous media: comparison of SPH simulations with micro-model experiments. Transp. Porous Media 114, 581–600.

Kutner, R., Masoliver, J., 2017. The continuous time random walk, still trendy: fifty-year history, state of art and outlook. Eur. Phys. J. B 90, 1–13.

Kuwata, Y., Suga, K., 2015. Anomaly of the lattice Boltzmann methods in three-dimensional cylindrical flows. J. Comput. Phys. 280, 563–569.

Ladd, A.J., Szymczak, P., 2021. Reactive flows in porous media: Challenges in theoretical and numerical methods. Annu. Rev. Chem. Biomol. Eng. 12, 543–571. doi:10.1146/annurev-chembioeng-092920-102703.

Lai, J., Wang, G., Wang, Z., Chen, J., Pang, X., Wang, S., Zhou, Z., He, Z., Qin, Z., Fan, X., 2018. A review on pore structure characterization in tight sandstones. Earth Sci. Rev. 177, 436–457.

Lam, C.N.C., Wu, R., Li, D., Hair, M.L., Neumann, A.W., 2002. Study of the advancing and receding contact angles: liquid sorption as a cause of contact angle hysteresis. Adv. Colloid Interface Sci. 96, 169–191. doi:10.1016/S0001-8686(01)00080-X.

Lanetc, Z., Zhuravljov, A., Jing, Y., Armstrong, R.T., Mostaghimi, P., 2022. Coupling of pore network modelling and volume of fluid methods for multiphase flow in fractured media. Fuel 319, 123563.

Lastiwka, M., Basa, M., Quinlan, N.J., 2009. Permeable and non-reflecting boundary conditions in SPH. Int. J. Numer. Methods Fluids 61, 709–724.

Latva-Kokko, M., Rothman, D.H., 2005. Static contact angle in lattice Boltzmann models of immiscible fluids. Phys. Rev. E 72, 046701. doi:10.1103/PhysRevE.72.046701.

Le Borgne, T., Dentz, M., Bolster, D., Carrera, J., De Dreuzy, J.R., Davy, P., 2010. Non-fickian mixing: Temporal evolution of the scalar dissipation rate in heterogeneous porous media. Adv. Water Resour. 33, 1468–1475.

Le Borgne, T., Dentz, M., Villermaux, E., 2015. The lamellar description of mixing in porous media. J. Fluid Mech. 770, 458–498.

Leclaire, S., Abahri, K., Belarbi, R., Bennacer, R., 2016. Modeling of static contact angles with curved boundaries using a multiphase lattice Boltzmann method with variable density and viscosity ratios. Int. J. Numer. Methods Fluids 82, 451–470.

Leclaire, S., Parmigiani, A., Malaspinas, O., Chopard, B., Latt, J., 2017. Generalized three-dimensional lattice Boltzmann color-gradient method for immiscible two-phase pore-scale imbibition and drainage in porous media. Phys. Rev. E 95, 033306. doi:10.1103/PhysRevE.95.033306.

Lenormand, R., Touboul, E., Zarcone, C., 1988. Numerical models and experiments on immiscible displacements in porous media. J. Fluid Mech. 189, 165–187.

Li, L., Mei, R., Klausner, J.F., 2017. Lattice Boltzmann models for the convection-diffusion equation: D2q5 vs d2q9. Int. J. Heat Mass Transf. 108, 41–62.

Li, L., Peters, C.A., Celia, M.A., 2006. Upscaling geochemical reaction rates using pore-scale network modeling. Adv. Water Resour. 29, 1351–1370.

Li, P., Berkowitz, B., 2018. Controls on interactions between resident and infiltrating waters in porous media. Adv. Water Resour. 121, 304–315.

Li, P., Berkowitz, B., 2019. Characterization of mixing and reaction between chemical species during cycles of drainage and imbibition in porous media. Adv. Water Resour. 130, 113–128.

Li, S., Raoof, A., Schotting, R., 2014. Solute dispersion under electric and pressure driven flows; pore scale processes. J. Hydrol. 517, 1107–1113.

Liu, C., Liu, Y., Kerisit, S., Zachara, J., 2015. Pore-scale process coupling and effective surface reaction rates in heterogeneous subsurface materials. Rev. Mineral. Geochem 80, 191–216.

Liu, H., Kang, Q., Leonardi, C.R., Schmieschek, S., Narvaez, A., Jones, B.D., Williams, J.R., Valocchi, A.J., Harting, J., 2016. Multiphase lattice Boltzmann simulations for porous media applications. Comput. Geosci. 20, 777–805. doi:10.1007/s10596-015-9542-3.

Liu, H., Valocchi, A.J., Kang, Q., Werth, C., 2013. Pore-scale simulations of gas displacing liquid in a homogeneous pore network using the lattice Boltzmann method. Transp. Porous Media 99, 555–580.

Liu, M., Shao, J., Chang, J., 2012. On the treatment of solid boundary in smoothed particle hydrodynamics. Sci. China Technol. Sci. 55, 244–254.

Liu, S., Zhang, C., Ghahfarokhi, R.B., 2021. A review of Lattice-Boltzmann models coupled with geochemical modeling applied for simulation of advanced waterflooding and enhanced oil recovery processes. Energy Fuels 35, 13535–13549. doi:10.1021/acs.energyfuels.1c01347.

Lu, B., Zhang, Y., Zheng, C., Green, C.T., O'Neill, C., Sun, H.G., Qian, J., 2018. Comparison of time nonlocal transport models for characterizing non-fickian transport: From mathematical interpretation to laboratory application. Water 10, 778.

Lunati, I., Jenny, P., 2006. Multiscale finite-volume method for compressible multiphase flow in porous media. J. Comput. Phys. 216, 616–636.

Maes, J., Geiger, S., 2018. Direct pore-scale reactive transport modelling of dynamic wettability changes induced by surface complexation. Adv. Water Resour. 111, 6–19. doi:10.1016/j.advwatres.2017.10.032.

Maes, J., Soulaine, C., 2018. A new compressive scheme to simulate species transfer across fluid interfaces using the volume-of-fluid method. Chem. Eng. Sci. 190, 405–418. doi:10.1016/j.ces.2018.06.026.

Markale, I., Cimmarusti, G.M., Britton, M.M., Jimenez-Martinez, J., 2021. Phase saturation control on mixing-driven reactions in 3D porous media. Environ. Sci. Technol. 55, 8742–8752.

Meakin, P., Tartakovsky, A.M., 2009. Modeling and simulation of pore-scale multiphase fluid flow and reactive transport in fractured and porous media. Rev. Geophys. 47.

Mehmani, A., Prodanović, M., 2014. The effect of microporosity on transport properties in porous media. Adv. Water Resour. 63, 104–119.

Mehmani, A., Verma, R., Prodanović, M., 2020. Pore-scale modeling of carbonates. Mar. Pet. Geol. 114, 104141.

Mehmani, Y., Anderson, T., Wang, Y., Aryana, S.A., Battiato, I., Tchelepi, H.A., Kovscek, A.R., 2021. Striving to translate shale physics across ten orders of magnitude: What have we learned? Earth Sci. Rev. 223, 103848.

Mehmani, Y., Balhoff, M.T., 2015a. Eulerian network modeling of longitudinal dispersion. Water Resour. Res. 51, 8586–8606.

Mehmani, Y., Balhoff, M.T., 2015b. Mesoscale and hybrid models of fluid flow and solute transport. Rev. Mineral. Geochem 80, 433–459.

Mehmani, Y., Oostrom, M., Balhoff, M.T., 2014. A streamline splitting pore-network approach for computationally inexpensive and accurate simulation of transp. porous media. Water Resour. Res. 50, 2488–2517.

Mehmani, Y., Tchelepi, H.A., 2017. Minimum requirements for predictive pore-network modeling of solute transport in micromodels. Adv. Water Resour. 108, 83–98.

Meigel, F.J., Darwent, T., Bastin, L., Goehring, L., Alim, K., 2022. Dispersive transport dynamics in porous media emerge from local correlations. Nat. Commun. 13, 1–9.

Meng, X., Yang, D., 2019. Pore-network modeling of particle dispersion in porous media. Colloids Surf. A Physicochem. Eng. Asp. 580, 123768.

Miao, X., Gerke, K.M., Sizonenko, T.O., 2017. A new way to parameterize hydraulic conductances of pore elements: A step towards creating pore-networks without pore shape simplifications. Adv. Water Resour. 105, 162–172.

Molaeimanesh, G.R., Akbari, M.H., 2016. Role of wettability and water droplet size during water removal from a pemfc gdl by lattice Boltzmann method. Int. J. Hydrog. Energy 41, 14872–14884. doi:10.1016/j.ijhydene.2016.06.252.

Monaghan, J.J., 1994. Simulating free surface flows with SPH. J. Comput. Phys. 110, 399–406.

Monaghan, J.J., 2005. Smoothed particle hydrodynamics. Rep. Prog. Phys. 68, 1703–1759. doi:10.1088/0034-4885/68/8/r01.

Montellá, E.P., Yuan, C., Chareyre, B., Gens, A., 2020. Hybrid multi-scale model for partially saturated media based on a pore network approach and lattice Boltzmann method. Adv. Water Resour. 144, 103709.

Morris, J.P., Fox, P.J., Zhu, Y., 1997. Modeling low reynolds number incompressible flows using SPH. J. Comput. Phys. 136, 214–226.

Muljadi, B.P., Blunt, M.J., Raeini, A.Q., Bijeljic, B., 2016. The impact of porous media heterogeneity on non-darcy flow behaviour from pore-scale simulation. Adv. Water Resour. 95, 329–340.

Nazari, F., Farajzadeh, R., Niasar, V.J., 2022. Critical parameters controlling wettability in hydrogen underground storage-an analytical study. JCIS Open 8, 100063.

Neuman, S.P., Tartakovsky, D.M., 2009. Perspective on theories of non-fickian transport in heterogeneous media. Adv. Water Resour. 32, 670–680.

Nissan, A., Berkowitz, B., 2019. Anomalous transport dependence on peclet number, porous medium heterogeneity, and a temporally varying velocity field. Phys. Rev. E 99, 033108.

Nissan, A., Dror, I., Berkowitz, B., 2017. Time-dependent velocity-field controls on anomalous chemical transp. porous media. Water Resour. Res. 53, 3760–3769.

Noetinger, B., Roubinet, D., Russian, A., Le Borgne, T., Delay, F., Dentz, M., De Dreuzy, J.R., Gouze, P., 2016. Random walk methods for modeling hydrodynamic transport in porous and fractured media from pore to reservoir scale. Transp. Porous Media 115, 345–385.

Noughabi, R.S., Mansouri, S.H., Raoof, A., 2023. Interface-induced dispersion in the unsaturated porous media: a pore-scale perspective. Adv. Water Resour. , 104474.

Nützmann, G., Maciejewski, S., Joswig, K., 2002. Estimation of water saturation dependence of dispersion in unsaturated porous media: experiments and modelling analysis. Adv. Water Resour. 25, 565–576.

Oostrom, M., Mehmani, Y., Romero-Gomez, P., Tang, Y., Liu, H., Yoon, H., Kang, Q., Joekar-Niasar, V., Balhoff, M., Dewers, T., et al., 2016. Pore-scale and continuum simulations of solute transport micromodel benchmark experiments. Comput. Geosci. 20, 857–879.

Padilla, I.Y., Yeh, T.C.J., Conklin, M.H., 1999. The effect of water content on solute transport in unsaturated porous media. Water Resour. Res. 35, 3303–3313.

Pavuluri, S., Maes, J., Doster, F., 2018. Spontaneous imbibition in a microchannel: analytical solution and assessment of volume of fluid formulations. Microfluid. Nanofluidics 22, 90. doi:10.1007/s10404-018-2106-9.

Peng, C., Xu, G., Wu, W., Yu, H.s., Wang, C., 2017. Multiphase SPH modeling of free surface flow in porous media with variable porosity. Comput. Geotech. 81, 239–248.

Peyman, M., Apostolos, K., 2016. Modelling two-phase flow in multi-mineral porous media using coupled level set-volume of fluid (CLSVOF) method. Proceedings of the GeoConvention .

Picchi, D., Battiato, I., 2018. The impact of pore-scale flow regimes on upscaling of immiscible two-phase flow in porous media. Water Resour. Res. 54, 6683–6707.

Popinet, S., 2018. Numerical models of surface tension. Annu. Rev. Fluid Mech. 50, 49–75.

Primkulov, B.K., Talman, S., Khaleghi, K., Shokri, A.R., Chalaturnyk, R., Zhao, B., MacMinn, C.W., Juanes, R., 2018. Quasistatic fluid-fluid displacement in porous media: Invasion-percolation through a wetting transition. Phys. Rev. Fluids 3, 104001.

Primkulov, B.K., Zhao, B., MacMinn, C.W., Juanes, R., 2022. Avalanches in strong imbibition. Communications Physics 5, 1–6.

Puyguiraud, A., Gouze, P., Dentz, M., 2021. Pore-scale mixing and the evolution of hydrodynamic dispersion in porous media. Phys. Rev. Lett. 126, 164501.

Qiao, C., Xu, Y., Zhao, W., Qian, J., Wu, Y., Sun, H., 2020. Fractional derivative modeling on solute non-fickian transport in a single vertical fracture. Frontiers in Physics , 378.

Qin, Z., Esmaeilzadeh, S., Riaz, A., Tchelepi, H.A., 2020. Two-phase multiscale numerical framework for modeling thin films on curved solid surfaces in porous media. J. Comput. Phys. 413, 109464.

Rabbani, A., Babaei, M., 2019. Hybrid pore-network and lattice-Boltzmann permeability modelling accelerated by machine learning. Adv. Water Resour. 126, 116–128.

Rabbani, H.S., Joekar-Niasar, V., Pak, T., Shokri, N., 2017. New insights on the complex dynamics of two-phase flow in porous media under intermediate-wet conditions. Sci. Rep. 7, 4584. doi:10.1038/s41598-017-04545-4.

Rabbani, H.S., Joekar-Niasar, V., Shokri, N., 2016. Effects of intermediate wettability on entry capillary pressure in angular pores. J. Colloid Interface Sci. 473, 34–43. doi:https://doi.org/10.1016/j.jcis.2016.03.053.

Rabbani, H.S., Or, D., Liu, Y., Lai, C.Y., Lu, N.B., Datta, S.S., Stone, H.A., Shokri, N., 2018. Suppressing viscous fingering in structured porous media. Proc. Natl. Acad. Sci. 115, 4833–4838. doi:10.1073/pnas.1800729115.

Rabbani, H.S., Seers, T.D., 2019. Inertia controlled capillary pressure at the juncture between converging and uniform channels. Sci. Rep. 9, 13870. doi:10.1038/s41598-019-49588-x.

Raeini, A.Q., Blunt, M.J., Bijeljic, B., 2012. Modelling two-phase flow in porous media at the pore scale using the volume-of-fluid method. J. Comput. Phys. 231, 5653–5668. doi:10.1016/j.jcp.2012.04.011.

Rahmat, A., Yildiz, M., 2018. A multiphase ISPH method for simulation of droplet coalescence and electro-coalescence. Int. J. Multiph. Flow 105, 32–44.

Ramstad, T., Berg, C.F., Thompson, K., 2019. Pore-scale simulations of single- and two-phase flow in porous media: Approaches and applications. Transp. Porous Media 130, 77–104. doi:10.1007/s11242-019-01289-9.

Ramstad, T., Hansen, A., 2006. Cluster evolution in steady-state two-phase flow in porous media. Phys. Rev. E 73, 026306. doi:10.1103/PhysRevE.73.026306.

Raoof, A., Hassanizadeh, S., 2013. Saturation-dependent solute dispersivity in porous media: pore-scale processes. Water Resour. Res. 49, 1943–1951.

Ren, W., E, W., 2007. Boundary conditions for the moving contact line problem. Phys. Fluids 19, 022101. doi:10.1063/1.2646754.

Riaud, A., Zhao, S., Wang, K., Cheng, Y., Luo, G., 2014. Lattice-Boltzmann method for the simulation of multiphase mass transfer and reaction of dilute species. Phys. Rev. E 89, 053308.

Roman, S., Abu-Al-Saud, M.O., Tokunaga, T., Wan, J., Kovscek, A.R., Tchelepi, H.A., 2017. Measurements and simulation of liquid films during drainage displacements and snap-off in constricted capillary tubes. J. Colloid Interface Sci. 507, 279–289.

Roubinet, D., Tartakovsky, D.M., 2013. Hybrid modeling of heterogeneous geochemical reactions in fractured porous media. Water Resour. Res. 49, 7945–7956.

Ryan, E.M., Tartakovsky, A.M., Amon, C., 2011. Pore-scale modeling of competitive adsorption in porous media. J. Contam. Hydrol. 120, 56–78.

Sahimi, M., 2011. Flow and Transp. Porous Media and fractured rock: from classical methods to modern approaches. John Wiley & Sons.

Sahimi, M., 2012. Dispersion in porous media, continuous-time random walks, and percolation. Phys. Rev. E 85, 016316.

Sato, T., Tanahashi, H., Loáiciga, H.A., 2003. Solute dispersion in a variably saturated sand. Water Resour. Res. 39.

Scheibe, T.D., Murphy, E.M., Chen, X., Rice, A.K., Carroll, K.C., Palmer, B.J., Tartakovsky, A.M., Battiato, I., Wood, B.D., 2015a. An analysis platform for multiscale hydrogeologic modeling with emphasis on hybrid multiscale methods. Groundwater 53, 38–56.

Scheibe, T.D., Schuchardt, K., Agarwal, K., Chase, J., Yang, X., Palmer, B.J., Tartakovsky, A.M., Elsethagen, T., Redden, G., 2015b. Hybrid multiscale simulation of a mixing-controlled reaction. Adv. Water Resour. 83, 228–239.

Seetha, N., Raoof, A., Kumar, M.M., Hassanizadeh, S.M., 2017. Upscaling of nanoparticle transp. porous media under unfavorable conditions: Pore scale to darcy scale. J. Contam. Hydrol. 200, 1–14.

Shams, M., Raeini, A.Q., Blunt, M.J., Bijeljic, B., 2018. A numerical model of two-phase flow at the micro-scale using the volume-of-fluid method. J. Comput. Phys. 357, 159–182.

Shan, X., Chen, H., 1993. Lattice Boltzmann model for simulating flows with multiple phases and components. Phys. Rev. E 47, 1815.

Shan, X., Chen, H., 1994. Simulation of nonideal gases and liquid-gas phase transitions by the lattice Boltzmann equation. Phys. Rev. E 49, 2941.

Singh, K., Bultreys, T., Raeini, A.Q., Shams, M., Blunt, M.J., 2022. New type of pore-snap-off and displacement correlations in imbibition. J. Colloid Interface Sci. 609, 384–392.

Soulaine, C., Maes, J., Roman, S., 2021a. Computational microfluidics for geosciences. Front. Water 3. doi:10.3389/frwa.2021.643714.

Soulaine, C., Pavuluri, S., Claret, F., Tournassat, C., 2021b. porousmedia4foam: Multi-scale open-source platform for hydro-geochemical simulations with OpenFOAM®. Environmental Modelling & Software 145, 105199.

Soulaine, C., Tchelepi, H.A., 2016. Micro-continuum approach for pore-scale simulation of subsurface processes. Transp. Porous Media 113, 431–456.

Sui, Y., Ding, H., Spelt, P.D., 2014. Numerical simulations of flows with moving contact lines. Annu. Rev. Fluid Mech. 46, 97–119. doi:10.1146/annurev-fluid-010313-141338.

Sullivan, S., Sani, F., Johns, M., Gladden, L., 2005. Simulation of packed bed reactors using lattice Boltzmann methods. Chem. Eng. Sci. 60, 3405–3418.

Sun, Y., Kharaghani, A., Tsotsas, E., 2016. Micro-model experiments and pore network simulations of liquid imbibition in porous media. Chem. Eng. Sci. 150, 41–53.

Swift, M.R., Orlandini, E., Osborn, W., Yeomans, J., 1996. Lattice Boltzmann simulations of liquid-gas and binary fluid systems. Phys. Rev. E 54, 5041.

Tahmasebi, P., Kamrava, S., 2018. Rapid multiscale modeling of flow in porous media. Phys. Rev. E 98, 052901.

Tartakovsky, A.M., Meakin, P., 2006. Pore scale modeling of immiscible and miscible fluid flows using smoothed particle hydrodynamics. Adv. Water Resour. 29, 1464–1478.

Tartakovsky, A.M., Meakin, P., Scheibe, T.D., West, R.M.E., 2007a. Simulations of reactive transport and precipitation with smoothed particle hydrodynamics. J. Comput. Phys. 222, 654–672.

Tartakovsky, A.M., Meakin, P., Scheibe, T.D., Wood, B.D., 2007b. A smoothed particle hydrodynamics model for reactive transport and mineral precipitation in porous and fractured porous media. Water Resour. Res. 43.

Tartakovsky, A.M., Meakin, P., Ward, A.L., 2009. Smoothed particle hydrodynamics model of non-aqueous phase liquid flow and dissolution. Transp. Porous Media 76, 11–34.

Tartakovsky, A.M., Trask, N., Pan, K., Jones, B., Pan, W., Williams, J.R., 2016. Smoothed particle hydrodynamics and its applications for multiphase flow and reactive transp. porous media. Comput. Geosci. 20, 807–834.

Tecklenburg, J., Neuweiler, I., Carrera, J., Dentz, M., 2016. Multi-rate mass transfer modeling of two-phase flow in highly heterogeneous fractured and porous media. Adv. Water Resour. 91, 63–77.

Tembely, M., Alameri, W.S., AlSumaiti, A.M., Jouini, M.S., 2020. Pore-scale modeling of the effect of wettability on two-phase flow properties for newtonian and non-newtonian fluids. Polymers 12, 2832.

TingYe, DingyiPan, CanHuang, MoubinLiu, 2019. Smoothed particle hydrodynamics (SPH) for complex fluid flows: Recent developments in methodology and applications. Phys. Fluids 31, 011301. doi:10.1063/1.5068697.

Tolke, J., Freudiger, S., Krafczyk, M., 2006. An adaptive scheme using hierarchical grids for lattice Boltzmann multi-phase flow simulations. Comput. Fluids 35, 820–830. doi:10.1016/j.compfluid.2005.08.010.

Triadis, D., Jiang, F., Bolster, D., 2019. Anomalous dispersion in pore-scale simulations of two-phase flow. Transp. Porous Media 126, 337–353.

Ursino, N., Gimmi, T., Flühler, H., 2001. Dilution of non-reactive tracers in variably saturated sandy structures. Adv. Water Resour. 24, 877–885.

Vanderborght, J., Vereecken, H., 2007. Review of dispersivities for transport modeling in soils. Vadose Zone J. 6, 29–52.

Vasilyev, L., Raoof, A., Nordbotten, J.M., 2012. Effect of mean network coordination number on dispersivity characteristics. Transp. Porous Media 95, 447–463.

Velásquez-Parra, A., Aquino, T., Willmann, M., Méheust, Y., Le Borgne, T., Jiménez-Martínez, J., 2022. Sharp transition to strongly anomalous transport in unsaturated porous media. Geophys. Res. Lett. 49, e2021GL096280.

Wang, J., Zhao, J., Zhang, Y., Wang, D., Li, Y., Song, Y., 2016a. Analysis of the effect of particle size on permeability in hydrate-bearing porous media using pore network models combined with ct. Fuel 163, 34–40.

Wang, Z., Chauhan, K., Pereira, J.M., Gan, Y., 2019. Disorder characterization of porous media and its effect on fluid displacement. Phys. Rev. Fluids 4, 034305.

Wang, Z.B., Chen, R., Wang, H., Liao, Q., Zhu, X., Li, S.Z., 2016b. An overview of smoothed particle hydrodynamics for simulating multiphase flow. Appl. Math. Model. 40, 9625–9655. doi:https://doi.org/10.1016/j.apm.2016.06.030.

Watson, F., Maes, J., Geiger, S., Mackay, E., Singleton, M., McGravie, T., Anouilh, T., Jobe, T.D., Zhang, S., Agar, S., Ishutov, S., Hasiuk, F., 2019. Comparison of flow and transport experiments on 3D printed micromodels with direct numerical simulations. Transp. Porous Media 129, 449–466. doi:10.1007/s11242-018-1136-9.

Wilkinson, D., Willemsen, J., 1983. Invasion percolation: a new form of percolation theory. J. Phys. A 16, 3365–3376.

Wu, D.S., Hu, R., Lan, T., Chen, Y.F., 2021. Role of pore-scale disorder in fluid displacement: Experiments and theoretical model. Water Resour. Res. 57, e2020WR028004. doi:10.1029/2020WR028004.

Wu, S., Rubinato, M., Gui, Q., 2020. SPH simulation of interior and exterior flow field characteristics of porous media. Water 12, 918.

Xiong, Q., Baychev, T.G., Jivkov, A.P., 2016. Review of pore network modelling of porous media: Experimental characterisations, network constructions and applications to reactive transport. J. Contam. Hydrol. 192, 101–117. doi:10.1016/j.jconhyd.2016.07.002.

Xu, K., Liang, T., Zhu, P., Qi, P., Lu, J., Huh, C., Balhoff, M., 2017a. A 2.5-D glass micromodel for investigation of multi-phase flow in porous media. Lab Chip 17, 640–646. doi:10.1039/C6LC01476C.

Xu, Z., Liu, H., Valocchi, A.J., 2017b. Lattice Boltzmann simulation of immiscible two-phase flow with capillary valve effect in porous media. Water Resour. Res. 53, 3770–3790. doi:10.1002/2017WR020373.

Yang, G., Rao, D., Cai, G., Zhou, R., 2021a. A discrete scheme of the fluid motion equation based on the pore-scale SPH method. AIP Adv. 11, 075102.

Yang, Q., Yao, J., Huang, Z., Zhu, G., Liu, L., Song, W., 2020. Pore-scale investigation of petrophysical fluid behaviours based on multiphase SPH method. J. Pet. Sci. Eng. 192, 107238.

Yang, X., Mehmani, Y., Perkins, W.A., Pasquali, A., Schönherr, M., Kim, K., Perego, M., Parks, M.L., Trask, N., Balhoff, M.T., et al., 2016. Intercomparison of 3D pore-scale flow and solute transport simulation methods. Adv. Water Resour. 95, 176–189.

Yang, X., Sun, H., Yang, Y., Liu, Y., Li, X., 2021b. Recent progress in multi-scale modeling and simulation of flow and solute transp. porous media. Wiley Interdisciplinary Reviews: Water 8, e1561.

Yang, Y., Cai, S., Yao, J., Zhong, J., Zhang, K., Song, W., Zhang, L., Sun, H., Lisitsa, V., 2021c. Pore-scale simulation of remaining oil distribution in 3D porous media affected by wettability and capillarity based on volume of fluid method. Int. J. Multiph. Flow 143, 103746.

Yin, X., Zhang, J., 2012. An improved bounce-back scheme for complex boundary conditions in lattice Boltzmann method. J. Comput. Phys. 231, 4295–4303.

Yoon, H., Kang, Q., Valocchi, A.J., 2015. Lattice Boltzmann-based approaches for pore-scale reactive transport. Rev. Mineral. Geochem 80, 393–431.

Zhang, C., Kaito, K., Hu, Y., Patmonoaji, A., Matsushita, S., Suekane, T., 2021. Influence of stagnant zones on solute transport in heterogeneous porous media at the pore scale. Phys. Fluids 33, 036605.

Zhang, D., Li, S., Jiao, S., Shang, Y., Dong, M., 2019. Relative permeability of three immiscible fluids in random porous media determined by the lattice Boltzmann method. Int. J. Heat Mass Transf. 134, 311–320. doi:10.1016/j.ijheatmasstransfer.2019.01.023.

Zhang, Y., Benson, D.A., 2008. Lagrangian simulation of multidimensional anomalous transport at the made site. Geophys. Res. Lett. 35.

Zhang, Y., Benson, D.A., Reeves, D.M., 2009. Time and space nonlocalities underlying fractional-derivative models: Distinction and literature review of field applications. Adv. Water Resour. 32, 561–581.

Zhang, Y., Meerschaert, M.M., Packman, A.I., 2012. Linking fluvial bed sediment transport across scales. Geophys. Res. Lett. 39.

Zhao, B., MacMinn, C.W., Primkulov, B.K., Chen, Y., Valocchi, A.J., Zhao, J., Kang, Q., Bruning, K., McClure, J.E., Miller, C.T., Fakhari, A., Bolster, D., Hiller, T., Brinkmann, M., Cueto-Felgueroso, L., Cogswell, D.A., Verma, R., Prodanovic, M., Maes, J., Geiger, S., Vassvik, M., Hansen, A., Segre, E., Holtzman, R., Yang, Z., Yuan, C., Chareyre, B., Juanes, R., 2019. Comprehensive comparison of pore-scale models for multiphase flow in porous media. Proc. Natl. Acad. Sci. 116, 13799–13806. doi:10.1073/pnas.1901619116.

1374 Zhao, S., Riaud, A., Luo, G., Jin, Y., Cheng, Y., 2015. Simulation of liquid mixing inside micro-
1375 droplets by a lattice Boltzmann method. Chem. Eng. Sci. 131, 118–128.

1376 Zhao, X., Sang, Q., Ma, J., Sarma, H., Dong, M., 2021. Method of determining the cohesion and
1377 adhesion parameters in the shan-chen multicomponent multiphase lattice Boltzmann models.
1378 Comput. Fluids 222, 104925.

1379 Zhou, L., Qu, Z.G., Chen, L., Tao, W.Q., 2015. Lattice Boltzmann simulation of gas–solid adsorp-
1380 tion processes at pore scale level. J. Comput. Phys. 300, 800–813.

1381 Zhu, Y., Fox, P.J., 2001. Smoothed particle hydrodynamics model for diffusion through porous
1382 media. Transp. Porous Media 43, 441–471.

1383 Zhu, Y., Fox, P.J., 2002. Simulation of pore-scale dispersion in periodic porous media using
1384 smoothed particle hydrodynamics. J. Comput. Phys. 182, 622–645.

1385 Zhuang, L., Raoof, A., Mahmoodlu, M.G., Biekart, S., de Witte, R., Badi, L., van Genuchten,
1386 M.T., Lin, K., 2021. Unsaturated flow effects on solute transp. porous media. J. Hydrol. 598,
1387 126301.